# Charmonium spectroscopy in strong magnetic fields by QCD sum rules: *S*-wave ground states

Sungtae Cho,[1,2,*] Koichi Hattori,[1,3,†] Su Houng Lee,[1,‡] Kenji Morita,[4,5,6,§] and Sho Ozaki[1,7,‖]

[1]*Institute of Physics and Applied Physics, Yonsei University, Seoul 120-749, Korea*
[2]*Division of Science Education, Kangwon National University, Chuncheon 200-701, Korea*
[3]*Theoretical Research Division, Nishina Center, RIKEN, Wako, Saitama 351-0198, Japan and RIKEN BNL Research Center, Bldg. 510A, Brookhaven National Laboratory, Upton, New York 11973, USA*
[4]*Frankfurt Institute for Advanced Studies, Ruth-Moufang-Str. 1, D-60438 Frankfurt am Main, Germany*
[5]*Institute of Theoretical Physics, University of Wroclaw, PL-50204 Wroclaw, Poland*
[6]*Yukawa Institute for Theoretical Physics, Kyoto University, Kyoto 606-8502, Japan*
[7]*Theory Center, IPNS, High energy accelerator research organization (KEK), 1-1 Oho, Tsukuba, Ibaraki 305-0801, Japan*

(Received 8 December 2014; published 19 February 2015)

We investigate quarkonium mass spectra in external constant magnetic fields by using QCD sum rules. We first discuss a general framework of QCD sum rules necessary for properly extracting meson spectra from current correlators computed in the presence of strong magnetic fields, that is, a consistent treatment of mixing effects caused in the mesonic degrees of freedom. We then implement operator product expansions for pseudoscalar and vector heavy-quark current correlators by taking into account external constant magnetic fields as operators and obtain mass shifts of the lowest-lying bound states $\eta_c$ and $J/\psi$ in the static limit with their vanishing spatial momenta. Comparing results from QCD sum rules with those from hadronic effective theories, we find that the dominant origin of mass shifts comes from a mixing between $\eta_c$ and $J/\psi$ with a longitudinal spin polarization, accompanied by other subdominant effects such as mixing with higher excited states and continua.

DOI: 10.1103/PhysRevD.91.045025 PACS numbers: 14.40.Pq, 21.65.Qr

## I. INTRODUCTION

It has been known for quite some time that external magnetic fields strongly interacting with charged fermions give rise to intriguing dynamics in vacuum, including not only nonlinear dynamics of photons within QED [1,2] but also an interplay with QCD. Motivated by formation of strong electromagnetic fields in neutron stars/magnetars [3,4] and ultrarelativistic heavy-ion collisions at the Relativistic Heavy Ion Collider (RHIC) and the Large Hadron Collider (LHC) [5–8], a number of lattice QCD simulations and analytic calculations have shown that strong magnetic fields modify properties of QCD vacuum such as quark condensates [5,9–18] and gluon condensates [19,20] and consequently modify even phase structures [15,19,21–23] and hadron properties [5,9,24–35]. One of the remarkable findings is a discrepancy between meson spectra obtained from a hadronic effective model calculation and a lattice QCD simulation in strong magnetic fields [26,27]. A lesson learned there might be the importance of studying bound-state properties on the basis of elementary degrees of freedom in the underlying theory, when the magnitudes of external fields approach and go beyond the typical scales of the theory. Especially in QCD, this is important not only because an internal structure of a bound state is changed but also because properties of QCD vacuum are changed. Therefore, these observations pose a fundamental question in QCD, i.e., how changes of QCD vacuum are reflected in meson spectra in external fields.

In a recent paper [34], we investigated a field theoretical approach to this issue and proposed a general framework of the QCD sum rules (QCDSR) applied to meson spectroscopy in external magnetic fields. This paper is supposed to be a detailed account of our framework providing a semianalytic method to elucidate the relation between properties of QCD vacuum and meson spectra in external magnetic fields. We also extend our detailed analysis to include the results for a transversely polarized $J/\psi$ with respect to the direction of the external field. Historically, the QCD sum rule was developed soon after the discovery of $J/\psi$ and first applied to heavy-quark systems [36–38]. The QCD sum rules remarkably predicted the small mass splitting between $\eta_c$ and $J/\psi$, which was subsequently confirmed by experiments [39]. The resolution in the results from the QCDSR was as high as the order of the mass splitting of less than 100 MeV. This was achieved by taking into account effects of a gluon condensate as well as a perturbative piece in current correlators on the basis of the operator product expansion (OPE) [40]. As shown in

*sungtae.cho@kangwon.ac.kr
†koichi.hattori@riken.jp
‡suhoung@yonsei.ac.kr
§kmorita@yukawa.kyoto-u.ac.jp
‖sho@post.kek.jp

 

the seminal papers [38,41,42], the QCD sum rules allow for manifestly incorporating nonperturbative effects of QCD vacuum through expectation values of operators in the OPE [43–45], which can be performed on an order-by-order basis with respect to mass dimensions of the operators and thus in a systematic manner. This structure in QCD sum rules indicates that we could investigate how changes in properties of QCD vacuum in the OPE manifest themselves in hadron properties in external environments. Indeed, the QCD sum rules at finite temperature/density [46–48] have been applied to heavy quarkonia [49–59], light mesons [60,61], and heavy-light mesons [62] in the last two decades and very recently those in strong external magnetic fields [33,34].

In particular, the heavy quarkonia have been investigated by various methods as well as the QCD sum rules, since dissociation of quarkonia in hot media with liberated color degrees of freedom, the so-called "$J/\psi$ suppression," was proposed as a signature of the quark-gluon plasma created in early times after the ultrarelativistic heavy-ion collisions [63,64]. Since then, not only the hot medium effects but also other effects, such as the cold nuclear matter effect, regeneration of melted charm quark pair, etc., have been examined in theoretical and experimental studies (see, e.g., Ref. [65] for reviews). While the strong electric and magnetic fields rapidly decay in the early-time dynamics [7], they could also act on heavy quarkonia and give rise to measurable effects [30,32] because estimates on heavy-quarkonium formation time indicate a prompt formation in early times [66] where the strong electromagnetic fields still persist with large magnitudes. Estimates on formation times given in Ref. [66] have shown that a significant fraction of charmonium and/or bottomonium produced in the heavy-ion collisions will be formed faster than 0.2 fm/c where the strength is still in the range from $0.1m_\pi^2$ to $m_\pi^2$ at RHIC energies.

Motivated by these theoretical and phenomenological aspects, we investigate $\eta_c$ and $J/\psi$ in the presence of external magnetic fields in detail by using hadronic effective theories and the QCD sum rules. While we focus on charmonia in this paper, the same methods can be applied to corresponding bottomonium states. We first give a systematic analysis of mixing patterns among charmonia in terms of a hadronic effective theory. We will find that only a mixing between a $\eta_c$ and a longitudinal $J/\psi$ is possible when charmonia are at rest, where a longitudinal $J/\psi$ is meant for a state with a vanishing spin component with respect to the direction of an external magnetic field. A level repulsion due to this mixing effect is consistent with results in a preceding study in terms of a potential model [32]. Bearing this in mind, we will switch to the QCD sum rules to investigate charmonia on the basis of the fundamental degrees of freedom and elaborate the hadronic spectral density Ansatz called the phenomenological side to consistently take into account the mixing effects [34]. We will show how to distinguish nonperturbative mass modifications from a level repulsion from the mixing effect that can be described on the hadronic basis. We note that our treatment of the mixing effects can be applied to general analyses on meson spectra in terms of correlation functions and should be applied to a very recent QCDSR analysis on $B$ mesons in strong magnetic fields [33] since the $B$ mesons are mixed with $B^*$ mesons. Our work demonstrates how to implement mixing effects in the QCDSR method, in particular for the heavy quark systems where both the OPE and the phenomenological side are well under control, and thus provides a general guideline to include mixing effects in approaches based on correlation functions.

Operator product expansion is then implemented up to dimension-4 operators in which we have external magnetic fields $\langle F_{\alpha\beta}F_{\mu\nu}\rangle$ as operator expectation values, in addition to a scalar gluon condensate $\langle G^a_{\mu\nu}G^{a\,\mu\nu}\rangle$ common to the OPE in the ordinary vacuum. It is noteworthy that the dominant effects in finite temperature/density come into the OPE only through dimension-4 gluon condensates that are related to the energy-momentum tensor of which the matrix elements are well estimated both at finite temperature from lattice QCD [51,52,55,56,58] and at normal nuclear matter density from measurements in deep inelastic scatterings [49]. Recently, it has also been shown that the strength of the charmonium wave function at the origin obtained from the QCDSR follows precisely that obtained from solving the Schrödinger equation with a finite temperature free energy potential extracted from lattice QCD [59]. In cases of external magnetic fields, it would become necessary to resum all-order terms with respect to dimensions of external fields $\langle FFF\cdots\rangle$ when the magnitude of a magnetic field goes beyond a separation scale in the OPE as recently performed for a vector current correlator [2].

Based on these elaborate treatments both on the phenomenological and the OPE sides, results of mass modification from the QCD sum rules are found to be consistent with those from the mixing effects with some slight discrepancies. We will then argue that the dispersion relation in the QCD sum rules is saturated by the mixing-induced terms and identify the mixing effect as the dominant origin of mass shifts of static $\eta_c$ and the longitudinal $J/\psi$. Then, we will examine effects of a perturbative heavy-quark loop as a subdominant origin of mass shifts in those states and of a transverse $J/\psi$ that is not involved in the mixing pattern.

This paper is organized as follows. We first examine possible mixing patterns in terms of a hadronic effective theory in Sec. II, followed by analyses with the use of the QCD sum rules in the subsequent sections. After a brief description of the QCD sum rule for heavy quarkonia in Sec. III, we elaborate on the phenomenological side bearing the mixing pattern in mind in Sec. IV and implement the OPE in the presence of an external magnetic field in Sec. V. Combining these ingredients, mass spectra of static $\eta_c$,

longitudinal $J/\psi$, and transverse $J/\psi$ from the QCD sum rule are obtained as shown in Sec. VI A with discussion about the role of mixing-induced terms on the phenomenological side and the origins of residual mass shift other than the mixing effect in Secs. VI B and VI C, respectively. Section VII is devoted to the summary. In the Appendix, we provide a list of the Wilson coefficients and some details of the calculations on the hadronic basis including calculation of the coupling constants in the mixing effects by using Bethe–Salpeter amplitudes of charmonia.

## II. MIXING EFFECTS IN EXTERNAL MAGNETIC FIELDS

We first examine effects of external magnetic fields on charmonia in terms of mesonic degrees of freedom. One should notice that even neutral mesons can be affected by external magnetic fields through effective interaction vertices and that any state can appear in the intermediate states as long as quantum numbers are matched. We thus investigate what mixing patterns are possible in external magnetic fields among the low-lying charmonia, $\eta_c$, $J/\psi$, $\chi_{c0}$, and $\chi_{c1}$. This can be systematically discussed in terms of a hadronic effective Lagrangian constrained by symmetries of the system as shown below.

We investigate mixing effects among the pseudoscalar ($\eta_c$), vector ($J/\psi$), scalar ($\chi_{c0}$), and axial-vector ($\chi_{c1}$) quarkonia by a hadronic effective Lagrangian approach. An effective Lagrangian includes all the relevant three-point vertices among two static quarkonia and a photon (external magnetic field),

$$\mathcal{L} = \mathcal{L}_{\mathrm{kin}+M} + \mathcal{L}_{\gamma\mathrm{PV}} + \mathcal{L}_{\gamma\mathrm{VA}} + \mathcal{L}_{\gamma\mathrm{SA}}, \tag{1}$$

where the kinetic and mass terms are as usual given by

$$\mathcal{L}_{\mathrm{kin}+M} = -\frac{1}{2}\partial_\mu P \partial^\mu P + \frac{1}{2} m_{\mathrm{P}}^2 P^2 - \frac{1}{2}\partial_\mu V_\nu \partial^\mu V^\nu + \frac{1}{2} m_{\mathrm{V}}^2 V^2 + (P \to S) + (V \to A). \tag{2}$$

The pseudoscalar and the vector fields are denoted by $P$ and $V^\mu$, respectively, and those terms for the scalar field ($S$) and the axial-vector field ($A^\mu$) are given by the replacements indicated in the last line. Possible interaction vertices among those fields, and thus mixing patterns, are informed from the Lorentz invariance and the parity and charge-conjugation symmetries. The vertices relevant for interactions among static charmonia are found to be

$$\mathcal{L}_{\gamma\mathrm{PV}} = \frac{g_{\mathrm{PV}}}{m_0} e\tilde{F}_{\mu\nu}(\partial^\mu P)V^\nu, \tag{3}$$

$$\mathcal{L}_{\gamma\mathrm{VA}} = i g_{\mathrm{VA}} e\tilde{F}_{\mu\nu} V^\mu A^\nu, \tag{4}$$

$$\mathcal{L}_{\gamma\mathrm{SA}} = \frac{g_{\mathrm{SA}}}{m_1} e\tilde{F}_{\mu\nu}(\partial^\mu S)A^\nu, \tag{5}$$

with $m_0 = (m_{\mathrm{P}} + m_{\mathrm{V}})/2$, $m_1 = (m_{\mathrm{S}} + m_{\mathrm{A}})/2$, and dimensionless effective coupling constants $g_{\mathrm{PV}}$, $g_{\mathrm{VA}}$, and $g_{\mathrm{SA}}$. These vertices are responsible for, e.g., radiative decay modes of quarkonia such as $J/\psi \to \eta_c + \gamma$.

Note that interaction vertices proportional to the field strength tensor $F^{\mu\nu}$, such as $\mathcal{L}_{\gamma\mathrm{VS}} \propto F_{\mu\nu}(\partial^\mu S)V^\nu$, do not play a role when addressing mixing effects among the static quarkonia in external magnetic fields and are not shown above. Since the field strength tensor $F^{\mu\nu}$ has finite elements only in the spatial components in case of an external magnetic field, it inevitably picks up vanishing spatial momenta of quarkonia when contracted with the derivatives, i.e., $F_{\mu\nu}\partial^\nu = 0$, and does not get involved in any mixing effect addressed here. Therefore, the interaction vertices should be proportional to the dual field strength tensor $\tilde{F}^{\mu\nu}$ as those in Eqs. (3)–(5). Note, however, that a coupling between the vector and axial-vector mesons (4) does not introduce any physical interaction, because the nonvanishing component of $\tilde{F}^{\mu\nu}$ picks up an unphysical temporal component of either the vector or axial-vector field.

Following from the discussions above, we eventually found that only two mixing patterns, one between $\eta_c$ and $J/\psi$ and the other between $\chi_{c0}$ and $\chi_{c1}$, are possible when they are at rest in external magnetic fields. These results are summarized in Table I. Since neither $\chi_{c0}$ nor $\chi_{c1}$ is mixed with $\eta_c$ and $J/\psi$, we shall focus on $\eta_c$ and $J/\psi$ in the present work and calculate the mass eigenstates in the presence of the mixing effects by solving equations of motion which follow from the effective Lagrangian (1) as

$$P\colon\ (\partial^2 + m_{\mathrm{P}}^2)P - \frac{g_{\mathrm{PV}}}{m_0} e\tilde{F}_{\alpha\beta}\partial^\alpha V^\beta = 0, \tag{6}$$

$$V\colon\ (\partial^2 + m_{\mathrm{V}}^2)V_\mu + \frac{g_{\mathrm{PV}}}{m_0} e\tilde{F}_{\alpha\mu}\partial^\alpha P = 0. \tag{7}$$

To show the mixing patterns more clearly, we hereafter assume that an external magnetic field is oriented in the positive $z$ direction, where the dual field strength tensor has only two nonzero components $\tilde{F}_{03} = -\tilde{F}_{30} = B$. In this configuration, the vector field reads $V^\mu = (V_0, \boldsymbol{V}_\perp, V_\parallel)$ where $V_0$, $\boldsymbol{V}_\perp$, and $V_\parallel$ denote the temporal, two transverse, and one longitudinal modes with respect to the external magnetic field, respectively.

TABLE I. Summary of possible mixing patterns for the quarkonia at rest in external magnetic fields. Subscripts denote longitudinal components of the vector and the axial-vector fields introduced in the text. Unless the components of the fields are indicated, the mixing effect is absent.

| | $\eta_c$ | $J/\psi$ | $\chi_{c0}$ | $\chi_{c1}$ |
|---|---|---|---|---|
| $\eta_c$ | — | $P - V_\parallel$ | – | – |
| $J/\psi$ | $V_\parallel - P$ | — | – | – |
| $\chi_{c0}$ | – | – | — | $S - A_\parallel$ |
| $\chi_{c1}$ | – | – | $A_\parallel - S$ | — |

With a vanishing spatial momentum $q^\mu = (\omega, 0, 0, 0)$, the equations of motion (6) and (7) result in a $2 \times 2$ matrix form:

$$\begin{pmatrix} -\omega^2 + m_{\rm P}^2 & -i\frac{g_{\rm PV}}{m_0}\omega eB \\ i\frac{g_{\rm PV}}{m_0}\omega eB & -\omega^2 + m_{\rm V}^2 \end{pmatrix} \begin{pmatrix} P \\ V_\parallel \end{pmatrix} = 0. \tag{8}$$

We notice that a mixing is held only between $\eta_c$ and the longitudinal $J/\psi$, and that the transverse $J/\psi$ is not mixed with $\eta_c$, as summarized in Table I. Following from the equations of motion (8), we obtain the physical mass eigenvalues in the presence of the mixing effect as

$$m^2_{J/\psi,\eta_c} = \frac{1}{2}\left( M_+^2 + \frac{\gamma^2}{m_0^2} \pm \sqrt{M_-^4 + \frac{2\gamma^2 M_+^2}{m_0^2} + \frac{\gamma^4}{m_0^4}} \right), \tag{9}$$

where $M_+^2 = m_{\rm P}^2 + m_{\rm V}^2$, $M_-^2 = m_{\rm V}^2 - m_{\rm P}^2$ and $\gamma = g_{\rm PV} eB$. Expanding Eq. (9) up to the second order in $\gamma$ and the leading order in $\frac{1}{2}(m_{\rm V} - m_{\rm P})/m_0$, we find

$$m^2_{J/\psi,\eta_c} = m^2_{\rm V,P} \pm \frac{\gamma^2}{M_-^2}, \tag{10}$$

with eigenvectors given by

$$\begin{aligned} |\eta_c)_B &= \left(1 - \frac{1}{2}\frac{\gamma^2}{M_-^4}\right)|P) - i\frac{\gamma}{M_-^2}|V), \\ |J/\psi)_B &= -i\frac{\gamma}{M_-^2}|P) + \left(1 - \frac{1}{2}\frac{\gamma^2}{M_-^4}\right)|V). \end{aligned} \tag{11}$$

We show plots of the mass shifts in the presence of the mixing effects in Fig. 1. The coupling constant $g_{\rm PV} = 2.095$ is here obtained by fitting the radiative decay widths measured in experiments. See Appendix A for details. We also show that the effective coupling between $\eta_c$ and $J/\psi$ can be obtained from the mixing amplitudes computed by utilizing Bethe–Salpeter amplitudes [67] and that the coupling strength agrees well with the one from the fitting method (see Appendix B 1). In Fig. 1, we find that the mass of $\eta_c$ decreases as $eB$ increases, while the mass of the longitudinal mode of $J/\psi$ (denoted by $J/\psi\|$) increases, indicating a level repulsion between these mass eigenstates in an external magnetic field. These behaviors are consistent with what was obtained in the potential-model approach [32], in which the authors found a level repulsion between $\eta_c$ and the longitudinal $J/\psi$ by solving Schrödinger equations in the presence of an external magnetic field.

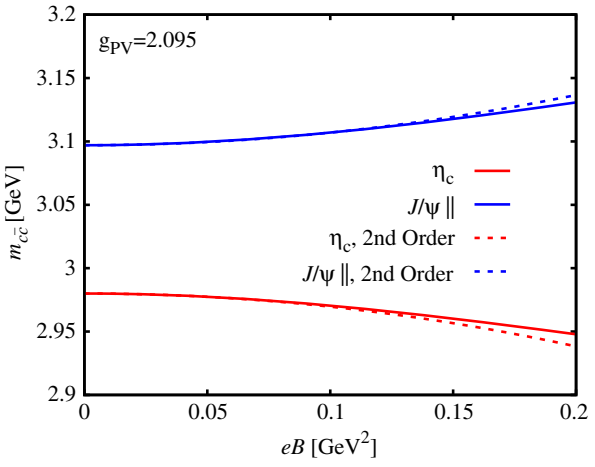


FIG. 1 (color online). Mixing effects between static $\eta_c$ and the longitudinal $J/\psi$. Solid (dotted) lines show a level repulsion from the mixing effects in all orders (second order) with respect to $eB$.

The mixing effect found above, however, does not exhaust possible effects of external magnetic fields on charmonia. Since the Lagrangian (1) contains only the minimal couplings to external magnetic fields, further mass shifts could be caused by magnetic fields acting on the loops and/or interactions among charmonia and more than two photons (magnetic fields) as higher-order corrections to the effective vertex (3). As for the loops effects, there could be fermion loops with light nucleons (nucleon-antinucleon loop) or with charmed baryons and boson loops with light or charmed mesons. Among those, the loops with light hadrons are highly suppressed due to the OZI rule. The only relevant loop effects are those from charmed mesons such as the $\bar{D}D$ loops, so we will examine effects of the loop contribution composed of charm quarks by the potential Nonrelativistic QCD (pNRQCD) approach in Sec. VI C. To investigate effects of those residual interactions as well as the mixing effect, we will in the next section switch to the QCDSR method based on the fundamental degrees of freedom.

## III. GENERALITIES IN QCD SUM RULE FOR HEAVY QUARKONIA

We provide a concise description of the QCD sum rule in application to quarkonium spectroscopy [38,41–43] used to investigate mass spectra of $\eta_c$ and $J/\psi$ in the present paper. Those charmonium states are respectively created by heavy-quark currents,

$$j^P = i\bar{c}\gamma^5 c \tag{12}$$

$$j^V_\mu = \bar{c}\gamma_\mu c, \tag{13}$$

where superscripts $P$ and $V$ denote pseudoscalar and vector currents, respectively. While one can construct a sum rule for the each channel, the following descriptions are common to all of these channels.

Since we investigate charmonia created by the currents (12) and (13), we should closely look at intermediate states in a current correlator,

$$\Pi^J(q) = i\int d^4x\, e^{iq\cdot x}\langle 0|T[J(x)J(0)]|0\rangle, \tag{14}$$

where superscripts $J$ denote a channel and the Lorentz indices in the vector current are suppressed for simplicity. While an imaginary part of the correlator is related to charmonium spectra, computation of this quantity is by no means easily attainable for an external momentum in the hadron mass scale, where the system is governed by nonperturbative effects of QCD in the strong-coupling regime. On the other hand, the asymptotic freedom in QCD allows for a series representation by OPE [40] with an external hard momentum $Q^2 = -q^2 \gg \Lambda^2_{\rm QCD}$ as

$$\Pi^J(Q^2) = C^J_{\rm p} \cdot \mathbf{1} + \sum_d C^{J(d)}(Q^2) \cdot \langle \mathcal{O}^{(d)} \rangle, \qquad (15)$$

where a summation index $d$ corresponds to the mass dimension of operators $\mathcal{O}$. The first term $C^J_{\rm p}$ being proportional to unit operator contains not only the leading-order diagram, i.e., the bare polarization diagram, but also perturbative corrections with respect to a small value of the QCD coupling constant $\alpha_s(Q^2) \ll 1$. The subsequent terms contain nonperturbative corrections, in which the Wilson coefficients $C^{J(d)}(Q^2)$ account for the hard-scale dynamics on the basis of a perturbative expansion while expectation values of the operators $\langle \mathcal{O}^{(d)} \rangle$ incorporate the soft-scale dynamics [40]. When quarks and gluons carry soft momenta in the intermediate states in the correlator, the expectation values of the operators such as the quark condensates $\langle \bar{q}q \rangle$ and the gluon condensates $\langle G^a_{\mu\nu} G^{a\,\mu\nu} \rangle$ are necessary for taking into account nonperturbative interactions with the QCD vacuum [37,38].

The OPE works efficiently when there is a definite separation scale, which usually resorts to an external hard momentum $Q^2$. The Wilson coefficient for a dimension $d$ operator behaves as a negative-power factor $C^{J(d)} \sim (Q^2)^{-d/2}$, and thus contributions of the higher-dimensional operators containing nonperturbative corrections are suppressed by $(Q^2)^{-d/2}$ as the momentum scale goes to the deep Euclidean region, $Q^2 \to \infty$, leaving perturbative corrections in the first term in Eq. (15). In case of a heavy-quark system, it was argued that the Wilson coefficient scales as $(4m^2 + Q^2)^{-d/2}$ [53,68]. The OPE is reliable even for a small value of $Q^2$ since any positive $Q^2$ in the complex $Q^2$ plane is distant from singularities originated from physical degrees of freedom, i.e., poles and thresholds of continua, owing to the large value of heavy-quark mass $m$. As long as expectation values of dimension-$d$ operators are much smaller than the separation scale $(4m^2 + Q^2)^{-d/2}$, one could plausibly perform the OPE. This is the case for the OPE in the presence of external magnetic fields expected for the early stage in relativistic heavy ion collisions. Up to the Large Hadron Collider energies, the magnetic field $|e\boldsymbol{B}| \lesssim 10 m_\pi^2$ can be induced by colliding nuclei [7], and thus it satisfies a condition $|e\boldsymbol{B}| \ll 4m^2 + Q^2$. We will implement the OPE in Secs. V A and V B.

Once the series representation by OPE (15) is obtained, it can be related to the spectral density, namely the imaginary part of the correlator in the physical region ($q^2 > 0$), through a dispersion relation

$$\tilde{\Pi}^J(Q^2) = \frac{1}{\pi} \int_0^\infty \frac{{\rm Im}\tilde{\Pi}^J(s)}{s + Q^2} ds + ({\rm subtraction}). \qquad (16)$$

We have introduced a dimensionless current correlator $\tilde{\Pi}^J(Q^2)$ normalized as follows. The dispersion relation (16) is satisfied individually with respect to three polarization modes in the vector channel, so we will investigate spin-projected scalar correlators $\tilde{\Pi}^V = (\epsilon_\mu \Pi^{V\mu\nu} \epsilon_\nu)/q^2$ specified by polarization vectors $\epsilon^\mu$ as shown in Sec. V B. We will find a mass splitting among spin polarization states in external magnetic fields. As for the pseudoscalar channel, we have a dimensionless correlator $\tilde{\Pi}^{\rm P} = \Pi^{\rm P}/q^2$.

One would be still skeptical to the applicability of the dispersion relation (16) to mass spectroscopy of bound states, since the series representation by the OPE is related only to an integrated spectral density which includes contributions from not only all the poles but also continua as a mixture. However, note that the integrand in Eq. (16) is weighted around the lower boundary of the integral region for a positive value of $Q^2$, and higher-energy contribution to the integrand is suppressed as the integral variable $s$ goes to infinity. This trend becomes stronger if the denominator has a higher power, implying that the integral is eventually dominated by the contribution from the lowest bound state for a sufficiently large power. Therefore, we shall take derivatives on both sides of Eq. (16) to suppress the higher-energy contribution other than the lowet pole. Putting the moments of the left-hand side to be

$$M^J_n(Q^2) = \frac{1}{n!} \left( -\frac{d}{dQ^2} \right)^n \tilde{\Pi}^J(Q^2), \qquad (17)$$

we find *the moment sum rule* as

$$M^J_n(Q^2) = \frac{1}{\pi} \int_0^\infty \frac{{\rm Im}\tilde{\Pi}^J(s)}{(s + Q^2)^{n+1}} ds. \qquad (18)$$

The moment sum rule (18) was invoked to calculate charmonium masses, in which the integral in Eq. (18) was carefully examined and was indeed found to be dominated by the lowest pole contribution as the number of derivatives $n$ becomes large [38,42]. Since the Wilson coefficient for a dimension-$d$ operator in the OPE, scaling as $(Q^2)^{-d/2}$ or $(4m^2 + Q^2)^{-d/2}$, has stronger dependence on $Q^2$ than the lower dimension terms, we notice that contributions from higher-dimension operators, and thus nonperturbative effects, are enhanced as the number of derivatives becomes larger. These scaling behaviors with respect to $Q^2$ and $n$ are naturally expected, because the

dominant lowest pole contribution at large $n$ is attributed to nonperturbative effects while a smeared continuum is described on the basis of a perturbative picture.

The moments of the Wilson coefficients (17) were obtained first in a series of seminal papers [37,38], followed by intensive calculations [41,42,69,70]. The first attempt was made at $Q^2 = 0$ on the basis of an argument that a convergence of the OPE is, even with vanishing $Q^2$, supported by a large value of charm quark mass [37,38]. However, it was shown that a better convergence is achieved by taking a finite momentum square $Q^2 > 0$ [41,42] and further that contributions from the higher-dimension operators at a large value of $n$ can be suppressed only when $Q^2$ is finite [71]. Therefore, the momentum square $Q^2$ is preferred to be taken large. However, if the momentum square $Q^2$ is taken to be arbitrarily large at a fixed $n$, it spoils the separation of the lowest pole contribution in Eq. (18) because the integrand is equally suppressed over the whole integral region. This separation would be restored, if we take a larger $n$ as we take a large value of $Q^2$ so that a steeper behavior of the denominator puts a weight on the lowest pole contribution, whereas convergence of the OPE again becomes weaker for a large $n$ due to picking up strong $Q^2$ dependence of the Wilson coefficients for the higher-dimension operators in Eq. (17). Therefore, one has to manage to adjust $Q^2$ and $n$ so that the convergence of the OPE and the separation of the lowest pole contribution are compatible to each other.

This point would become rather clear if one takes simultaneous limits $Q^2 \to \infty$ and $n \to \infty$ while maintaining a constant ratio $M^2 := Q^2/n$. Following conventions in Ref. [72], we define the limiting form of the moments (17) as

$$\mathcal{M}^J_{\rm OPE}(M^2) = \lim_{\substack{Q^2,n\to\infty \\ Q^2/n=M^2}} \pi(Q^2)^{n+1} M^J_n(Q^2), \tag{19}$$

and then, taking the same limits on the right-hand side in Eq. (18), we find *the exponential or Borel sum rule*:

$$\mathcal{M}^J_{\rm OPE}(M^2) = \int {\rm Im}\tilde{\Pi}^J(s) e^{-\frac{s}{M^2}} ds. \tag{20}$$

Equation (19) expresses the Borel transform of the correlator, by which a term scaling as $(4m^2 + Q^2)^{-d} \cdot \langle \mathcal{O}^{(d)} \rangle$ in the OPE (15) is transformed to be $\{M^{(d-2)}(d/2-1)!\}^{-1} \langle \mathcal{O}^{(d)} \rangle e^{-4m^2/M^2}$. Therefore, the exponential sum rule (20) scales by the *Borel mass* $M^2$ as

$$\sum_d \frac{M^{-(d-2)}}{(d/2-1)!} \langle O^{(d)} \rangle \sim \int {\rm Im}\tilde{\Pi}^J(s) e^{-\frac{s-4m^2}{M^2}} ds. \tag{21}$$

Now, it is evident that the lowest pole contribution is efficiently separated owing to an exponential factor suppressing the excited states and continua for a small Borel mass $M^2$, whereas the series representation by the OPE is better convergent when $M^2$ is sufficiently large. The charmonium mass spectrum is reliably obtained from the QCDSR since one can find an intermediate band of the Borel mass $M^2$ called the "Borel window" in which the above requirements, convergence and separation, are compatible to each other [72]. Analysis of the Borel window in the exponential sum rule (20) is simpler and can be done in a more systematic way than those with the moment sum rule containing two parameters $Q^2$ and $n$. Note also that the Wilson coefficients are transformed to be suppressed by a factorial of the operator dimension $1/(d/2-1)!$, and thus the convergence of the OPE is improved. Therefore, we will use the exponential sum rule (20) in subsequent sections.

## IV. SPECTRAL ANSATZ IN THE PRESENCE OF MIXING EFFECTS [34]

As described in the last section, the current correlator (14) can be expressed in two ways: the OPE in the deep Euclidean region ($Q^2 = -q^2 \gg 1$) and the spectral density $\rho^J(s) = {\rm Im}\tilde{\Pi}^J(s)/\pi$ in the physical region ($q^2 > 0$). They are connected to each other through a dispersion relation (16). The right-hand side of Eq. (16) is conventionally called the "phenomenological side" because the spectral density is parametrized in hadronic degrees of freedom. The spectral density $\rho^J(s)$ is often assumed to have a perturbative continuum ${\rm Im}\tilde{\Pi}^J_{\rm pert}(s)/\pi$ and a single pole at the ground-state mass $\delta(s - m^2_{\rm pole})$. This Ansatz works sufficiently well when the ground-state pole is well separated from a threshold of continuum as only the low-energy structure is important for the exponential sum rule (20) owing to the exponential suppression of the higher-energy part of the spectral density by the Borel transformation. Thus, this simple Ansatz works well for the tightly bound ground-state charmonia. One should, however, be careful to this point in the presence of the magnetically induced mixing discussed in Sec. II, because it induces a $\eta_c$ (longitudinal $J/\psi$) pole in the longitudinal vector (pseudoscalar) current correlator. Therefore, there would appear two adjacent poles in the low-energy region around the ground-state pole, and they could contribute to the Borel-transformed correlator with the same order of magnitudes. We will find that an appropriate Ansatz in the presence of external magnetic fields has a form[1]

$$\rho^J(s) = \pi^{-1}[f_0 \delta(s - m^2_{c\bar{c}}) + \theta(s - s_0){\rm Im}\tilde{\Pi}^J_{\rm pert}(s) + {\rm Im}\tilde{\Pi}^{J,{\rm ext}}_{\rm ph}(s)], \tag{22}$$

[1]The "pole + continuum" part in the vector channel is assumed for a scalar part $\tilde{\Pi}^{\rm V}$ obtained from a spin projection by the polarization vectors (59) and (60) and the normalization specified below Eq. (16) as $q^{-2}\epsilon_\mu \Pi^{{\rm V},\mu\nu}\epsilon_\nu = q^{-2}\epsilon_\mu\epsilon_\nu(q^\mu q^\nu - q^2 g^{\mu\nu})\tilde{\Pi}^{\rm V} = \tilde{\Pi}^{\rm V}$ for a static charmonia.

where $f_0$ is a coupling strength between the heavy-quark current and the ground-state charmonium in vacuum which is related to the mass and electronic decay width and found to be $0.542\ \mathrm{GeV}^2$ for the vector current [42,59]. An effective threshold $s_0$ is fitted in the QCDSR analyses. The last term takes into account effects of magnetic fields as shown below.

We carefully examine the magnetically induced term $\mathrm{Im}\Pi^{J,\mathrm{ext}}_{\mathrm{ph}}(s)$ in the spectral Ansatz. While we will describe calculations for the pseudoscalar channel, the same calculations are straightforwardly applied to the longitudinal component in the vector channel. A low-energy expression of the pseudoscalar current correlator (14) in the second order of $eB$ is diagrammatically represented in Fig. 2. The first diagram, surviving in the vanishing field limit, corresponds to the ground-state pole in Eq. (22), which is the $\eta_c$ pole in case of the pseudoscalar channel. As shown by the other magnetically induced diagrams, we have not only an $\eta_c$ pole but also a longitudinal $J/\psi$ pole mixed into the pseudoscalar channel. One also finds that the longitudinal $J/\psi$ couples to the pseudoscalar current both *directly* and *indirectly*. A direct coupling is, as shown in Fig. 3, induced by a three-point vertex among a pseudoscalar current, an external magnetic field, and a longitudinal $J/\psi$. An indirect coupling is obtained by replacing the pseudoscalar current in the direct coupling by a $\eta_c$, resulting in the hadronic coupling (3) as already discussed. Thus, the second (third) diagram in Fig. 2 shows a process induced solely by the indirect (direct) couplings. Those contributions to the matrix element in Eq. (22) are given by

$$\Pi^{\mathrm{P,ext}}_{\mathrm{ph}}(q^2) = \frac{|\langle 0|J^5|J/\psi\rangle|^2}{q^2 - m^2_{J/\psi}}, \tag{23}$$

with the matrix elements

$$|\langle 0|J^5|J/\psi\rangle|^2 = f_{\mathrm{dir}} + f\frac{|\langle P|J/\psi\rangle|^2}{(q^2 - m^2_{\mathrm{P}})^2}, \tag{24}$$

where a direct-coupling strength between the pseudoscalar current and the longitudinal $J/\psi$ reads $f_{\mathrm{dir}} = |\langle V|J^5(q)|0\rangle|^2$ and a coupling strength between the pseudoscalar current and a $\eta_c$ is proportional to $f_0$ as $f = |\langle P|J^5(q)|0\rangle|^2 = f_0 \cdot m_0^2/\pi$. The effective vertex (3) leads to $|\langle P|J/\psi\rangle|^2 = \gamma^2$ for a static charmonium in the heavy-quark limit $m_0 \sim m_{\mathrm{P,V}}$. As shown in Fig. 3, one can calculate the direct-coupling strength $f_{\mathrm{dir}}$ from two triangle diagrams by using the Bethe–Salpeter amplitudes of the $S$-wave quarkonia [67]. Led by a diagramatic calculation performed in the heavy-quark limit in Appendix B 2, we find the direct-coupling strength as

$$f_{\mathrm{dir}} = \frac{a_0^4 Q_c^2}{64}(eB)^2 f, \tag{25}$$

with an electric charge of a charm quark $Q_c = 2/3$. The Bohr radius $a_0 = 0.811\ \mathrm{GeV}^{-1}$ is chosen to fit the root-mean-square radius of the $J/\psi$ obtained from the Cornell potential model [73]. Inserting Eq. (24) into Eq. (23), we find that the rhs in Eq. (23) can be decomposed as

$$\begin{aligned}\Pi^{\mathrm{P,ext}}_{\mathrm{ph}}(q^2) &= \frac{f\gamma^2}{(q^2 - m^2_{\mathrm{P}})^2(q^2 - m^2_{\mathrm{V}})} \\ &= \frac{f\gamma^2}{M_-^4}\left[\frac{1}{q^2 - m^2_{\mathrm{V}}} - \frac{1}{q^2 - m^2_{\mathrm{P}}} - \frac{M_-^2}{(q^2 - m^2_{\mathrm{P}})^2}\right],\end{aligned} \tag{26}$$

where notations are specified below Eq. (9). Before discussing physical meaning of these terms, there are some comments in order. First, one can replace the $J/\psi$ mass in the denominator by the vacuum mass $m_{\mathrm{V}}$ within the second-order corrections in $eB$, because the correlator (26) has explicit second-order corrections in the numerator.

As for the longitudinal $J/\psi$ pole induced by the direct-coupling term, we find that its strength is much smaller than the hadronic-coupling strength of the longitudinal $J/\psi$ pole in Eq. (26), because the direct-coupling strength (25) is proportional to the small value of the Bohr radius of tightly bound charmonia. A ratio of the direct-coupling strength over the hadronic-coupling strength in Eq. (26) is found to be

$$f_{\mathrm{dir}}/(f\gamma^2/M_-^4) \sim 0.0003, \tag{27}$$

so that one can safely neglect the contributions of the direct couplings. We also neglect cross-terms depicted by the last two diagrams in Fig. 2. Possible corrections to the direct-coupling strength in a higher order of $eB$ should be neglected in the present framework so that the correlator is consistently constructed within the second order in $eB$. Another possible correction might be a distortion of the $S$-wave wave function in an external strong magnetic field, while in the above calculation, we inserted the Coulombic wave function in the ordinary vacuum. However, because

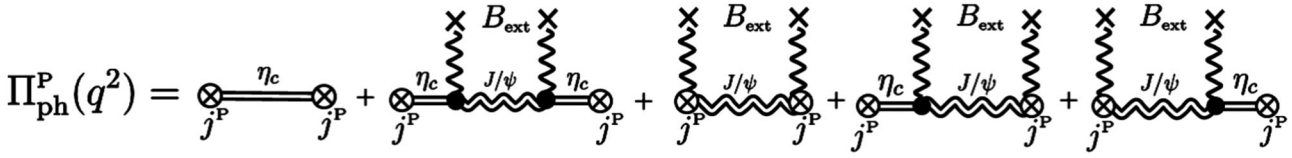


FIG. 2. Diagramatic representation of the phenomenological side for the pseudoscalar channel.

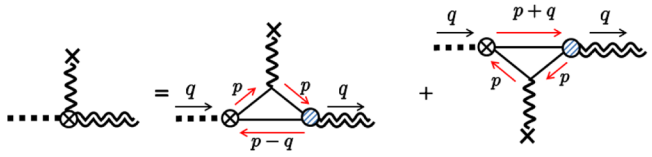


FIG. 3 (color online). A direct-coupling strength between the pseudoscalar (vector) current and $\eta_c$ ($J/\psi$) from triangle diagrams. Shaded vertices show form factors given by the Bethe–Salpeter amplitudes of the $S$-wave quarkonia (70) and (71), while vertices with crosses denote the currents.

of the small ratio (27), the modification of the wave function in strong magnetic fields would not be important, unless the wave function is very strongly distorted by the external magnetic fields. To estimate the order of this effect, we should compare the magnitudes of the Coulomb force in the potential model, $\kappa/r^2$, with that of an external magnetic field. With a strength of the Coulomb force $\kappa = 0.52$ from Ref. [73] and the Bohr radius $a_0 = 0.811$ GeV $\sim 0.16$ fm above, we have $eB/(\kappa/a_0^2) \sim 0.25$ even for the maximal strength $eB = 10m_\pi^2$ [7]. This estimate indicates that distortion of the Coulombic wave function by the external magnetic fields will be so small that we can still neglect the direct coupling under the modifications of the wave function in strong magnetic fields. Similarly, finite temperature/density effects in the heavy-ion collisions could act on the direct coupling. However, these effects would be also so small, basically because the strength $f_{\rm dir}$ is proportional to the Bohr radius $a_0$, while the mixing strength between $\eta_c$ and the longitudinal $J/\psi$ is independent of the Bohr radius. Even if the Bohr radius becomes ten times larger for charmonia melting in the hot medium, the ratio shown in Eq. (27) is still of order $10^{-3}$, so one can neglect the direct coupling compared to the hadronic mixing between $\eta_c$ and the longitudinal $J/\psi$.

To understand physical meaning of the terms in Eq. (26), it is instructive to compare them with the second-order perturbation theory performed in Sec. II. Note that, neglecting the direct couplings, the pseudoscalar current is first coupled to an $\eta_c$ in any process whether the intermediate state is an $\eta_c$ or $J/\psi$. Therefore, by using the coupling strength $f$, the current correlator may be written as

$$\Pi^{\rm P}_{\rm 2nd}(q^2) = f\left[\frac{|(P|\eta_c)_B|^2}{q^2 - m_{\eta_c}^2} + \frac{|(P|J/\psi)_B|^2}{q^2 - m_{J/\psi}^2}\right], \tag{28}$$

where physical masses $m_{\eta_c, J/\psi}$ and corresponding wave functions in the presence of the mixing effect have been obtained in Eqs. (10) and (11), respectively. Now we will find that all three terms in Eq. (26) follow from an expansion of the rhs in Eq. (28) up to the second order in $eB$. The first term in Eq. (26) corresponds to putting an intermediate $J/\psi$ state on mass-shell in the second diagram in Fig. 2. This is a production of an on-shell $J/\psi$ from the pseudoscalar current via off-shell $\eta_c$. The second term with a negative sign is necessary for a conservation of the normalization of the spectral density, because the coupling of $\eta_c$ to the current must be reduced to balance the occurrence of the coupling to $J/\psi$. These interpretations are confirmed by expanding the rhs in Eq. (28), because we obtain these two terms from overlaps between the properly normalized unperturbed and perturbed states, $|(P|\eta_c)_B|^2 \sim 1 - (\gamma/M_-^2)^2$ and $|(P|J/\psi)_B|^2 \sim (\gamma/M_-^2)^2$. To take into account the mixing effect with maintaining the normalization, one should include both single poles at $\eta_c$ and $J/\psi$ with the residues shown in Eq. (26), giving a two-peak structure in the spectral Ansatz. The third term has a double pole at the $\eta_c$ mass with a factor $M_-^2$ which gives an off-shellness of a virtual $J/\psi$ in the intermediate state. One finds that a virtual transition to $J/\psi$ between on-shell $\eta_c$ states is nothing but the origin of the mass shift due to the mixing effect. Correspondingly, this term comes from an expansion in Eq. (28) with respect to the mass correction of $\eta_c$ shown in Eq. (10). Therefore, we have found that, if the double-pole term is included on the phenomenological side, it balances the corresponding effect embedded on the OPE side performed on the basis of the fundamental degrees of freedom, and we will obtain a residual mass shift due to nonperturbative effects as a result of the QCD sum rule. On the other hand, if the double-pole term is not included, we will obtain a resultant mass shift due to the mixing effect and the residual effects. This observation enables us to separate the residual effects of magnetic fields from the mixing effect and extract effects of magnetic fields *not described in the hadronic level*. We will come back to this point in Secs. VI A and VI B with plots of mass shifts from QCD sum rules.

Let us perform the Borel transformation of the phenomenological side. Inserting the ground-state pole term in Eq. (22) into the rhs of Eq. (20), we simply find

$$\mathcal{M}^{\rm P,pole}_{\rm ph} = f_0 e^{-m_{\eta_c}^2/M^2}. \tag{29}$$

From the second term of Eq. (22), the Borel transformation of the perturbative continuum part is found to be

$$\mathcal{M}^{J,\rm cont}_{\rm ph} = \int_{s_0}^{\infty} ds e^{-s/M^2} {\rm Im}\tilde{\Pi}^{J,\rm pert}(s), \tag{30}$$

where the expression for the perturbative continuum ${\rm Im}\tilde{\Pi}^{J,\rm pert}(s)$ is given in Ref. [43]. By inserting the magnetically induced part (23) into the rhs of Eq. (20), we obtain

$$\mathcal{M}^{\rm P,ext}_{\rm ph}(M^2) = f_0(eB)^2\left[Q_c^2\frac{a_0^4}{64}e^{-\frac{m_{\rm V}^2}{M^2}} + \frac{g_{\rm PV}^2}{M_-^4}\left(e^{-\frac{m_{\rm V}^2}{M^2}} - e^{-\frac{m_{\rm P}^2}{M^2}} + \frac{M_-^2}{M^2}e^{-\frac{m_{\rm P}^2}{M^2}}\right)\right], \tag{31}$$

where $f_0 = \pi f/m_0^2$ with $1/m_0^2$ coming from the normalization of the correlator described below Eq. (16). A corresponding formula for the longitudinal $J/\psi$ can be obtained by interchanging $m_{\rm P}$ and $m_{\rm V}$ as

$$\mathcal{M}_{\rm ph}^{{\rm V}_\parallel,{\rm ext}}(M^2) = f_0(eB)^2\left[Q_c^2\frac{a_0^4}{64}e^{-\frac{m_{\rm P}^2}{M^2}} + \frac{g_{\rm PV}^2}{M_-^4}\left(-e^{-\frac{m_{\rm V}^2}{M^2}} + e^{-\frac{m_{\rm P}^2}{M^2}} - \frac{|M_-^2|}{M^2}e^{-\frac{m_{\rm V}^2}{M^2}}\right)\right]. \tag{32}$$

The first terms in Eqs. (31) and (32) are the direct-coupling terms in Eq. (24) which are, however, negligible as discussed above. Following from a sign flip in $M_-^2$, we find that the double-pole contribution in the vector channel has the opposite sign to that of the last term in Eq. (31).

One should remember that these magnetically induced terms on the phenomenological side are not applied to the transverse $J/\psi$, because any magnetically induced coupling in Fig. 2 is absent for the transverse component. Therefore, we will employ the conventional pole + continuum Ansatz for the transverse $J/\psi$.

These Ansätze on the phenomenological side will be used to extract the charmonium mass spectra in Sec. VI A, prior to which we need to examine the OPE in the next section.

## V. OPERATOR PRODUCT EXPANSION

In this section, we include effects of a constant external magnetic field into a series representation of the current correlator by the OPE (15). It should be noticed first that interactions between quarks and a constant magnetic field can be suitably regarded as a soft process, since a constant external field does not cause any momentum transfer to quarks in a vacuum polarization (see Fig. 4). A momentum transfer is exactly zero because of a translational invariance [74]. A constant magnetic field is thus treated as an operator expectation value in the OPE and gives rise to additional terms to a series in the ordinary vacuum. We compute the Wilson coefficients of these terms for an external magnetic field in Sec. V B, following a brief description of the OPE in the ordinary vacuum.

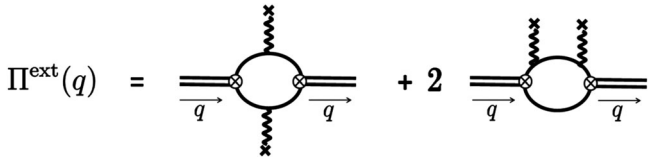


FIG. 4. Diagramatic representation of corrections by an external magnetic field. External fields and a one-loop perturbative part correspond to the operators $\langle F_{\alpha\beta}F_{\gamma\delta}\rangle$ and the Wilson coefficients $C^{\alpha\beta\gamma\delta}$ in Eq. (38), respectively.

### A. OPE for charmonia in the ordinary vacuum

The OPE for heavy-quark systems was examined in detail for the sake of investigating the lowest bound states created by the various currents [37,38,41,42]. As the higher-dimension terms in the OPE are suppressed by negative powers of the Borel mass and the factorial factors of the operator dimension [see Eq. (21)], a series representation in the OPE is saturated by the first few terms. Indeed, it was found that the vacuum charmonium mass spectra measured in experiments are reproduced by including the perturbative terms and the dimension-4 scalar gluon condensate [37,42,43,72]

$$\Pi_{\rm vac}^J(Q^2) \sim C_{\rm p}^J(Q^2)\cdot \boldsymbol{1} + C_{G_0}^J(Q^2)\cdot G_0, \tag{33}$$

where the superscripts $J$ denote a channel of the currents (12), (13). The correlator $\Pi_{\rm vac}^{\rm V}$ and the Wilson coefficients $C_{\rm p}^{\rm V}$ and $C_{G_0}^{\rm V}$ should have two Lorentz indices in the vector channel $J = V$. We, however, suppress those indices as well as the superscript $J$ for simplicity below as in Eq. (14). An expectation value of the scalar gluon condensate has a form $G_0 = \langle\frac{\alpha_s}{\pi}G^{a\mu\nu}G^a_{\mu\nu}\rangle$. Note that a heavy-quark condensate $\langle\bar{c}c\rangle$ does not contribute to the OPE (33) in the leading order of a heavy-quark expansion $\mathcal{O}(1/m)$, because it is canceled in an operator mixing with the gluon condensate [38,75] (see also Sec. 3.3.5 in Ref. [43] for a comprehensive description). Contributions from higher-dimension gluon condensates are small enough in the ordinary vacuum, giving stable Borel curves [71]. Such stability is maintained even at finite temperature up to around 1.1 times the QCD phase transition temperature [51]. The properties of charmonium extracted from such calculations have been recently shown to be consistent with that obtained by solving the Schrödinger equation with the free energy potential extracted from lattice calculations [59]. However, above this temperature, the contributions from higher-dimensional operators cannot be neglected [76], and a different resummation technique will be more appropriate to calculate the OPE [47]. In our present analysis, we include the terms up to the dimension-4 scalar gluon condensate as in Eq. (33) since recent studies have shown that effects of external magnetic fields on the gluon condensate is sufficiently small as briefly discussed below [19,20]. A summary of the Wilson coefficients is available in Refs. [43,70].

Following the definition of the moments (17), one can straightforwardly calculate the moments of the Wilson coefficients in Eq. (33). This has been carried out systematically in various channels [41,42], and explicit forms in their conventions are given by

$$M_n^{\rm vac} = A_n(1 + \alpha_s a_n + \phi_b b_n). \tag{34}$$

An overall factor $A_n$ corresponds to the leading-order perturbative term in the zeroth order of the QCD coupling

constant $g_s$. The second and third terms between the parentheses give the next-to-leading-order perturbative correction and the leading power correction by the scalar gluon condensate, which are respectively proportional to the fine structure constant in QCD, $\alpha_s = g_s^2/(4\pi)$, and the scalar gluon condensate,

$$\phi_b = \frac{4\pi^2 G_0}{9(4m^2)^2}. \tag{35}$$

These coefficients $A_n$, $a_n$, and $b_n$ are shown in Table 1 in Ref. [42].

A useful recipe for taking the simultaneous limits $Q^2, n \to \infty$ in Eq. (19) was provided in the Appendix of Ref. [72] with the help of a relation between special functions (see also Appendix C in this paper). Following the description therein, one obtains the Borel-transformed Wilson coefficients to be

$$\mathcal{M}^{\rm vac}(\nu) = \pi e^{-\nu} A(\nu)[1 + \alpha_s a(\nu) + \phi_b b(\nu)], \tag{36}$$

where a dimensionless inverse Borel mass is defined by $\nu = 4m^2/M^2$. The coefficients in Eq. (36) correspond to those denoted by the same alphabets in Eq. (34). Explicit forms of $A(\nu)$, $a(\nu)$, and $b(\nu)$ are summarized in appendixes of Refs. [55,72].

### B. OPE in external magnetic fields

We include effects of a constant external magnetic field into the OPE as an operator for the soft dynamics. Since the magnitude of external fields up to the LHC energy satisfies the condition $|e\boldsymbol{B}| \ll 4m^2 + Q^2$ discussed in Sec. III, the OPE in an external magnetic field is thus implemented as a sum of the conventional terms in the ordinary vacuum (33) and those from the external magnetic field shown in Fig. 4 as

$$\Pi(Q^2) = \Pi^{\rm vac}(Q^2) + \Pi^{\rm ext}(Q^2). \tag{37}$$

We first remark on a possible modification of the gluon condensate $\langle G^{a\mu\nu} G^a_{\mu\nu}\rangle$ in the vacuum part $\Pi^{\rm vac}(Q^2)$ caused by external magnetic fields. While the light-quark condensates in magnetic fields at zero temperature and density have been known to increase by a mechanism called "magnetic catalysis" [11,16], a similar growth of a gluon condensate at zero temperature and density was recently observed in both lattice QCD and analytic studies [19,20]. Modification of a gluon condensate should be small, since external magnetic fields do not directly couple to gluons but indirectly through sea quarks. Indeed, this modification is estimated to be less than 10% for a magnitude of external magnetic fields around and smaller than the pion mass squared $|e\boldsymbol{B}| \lesssim 10 m_\pi^2$. Thus, we do not take this into account in the present work performed at zero temperature and density, and effects of magnetic fields can be included as additional terms as in Eq. (37).

Those additional terms $\Pi^{\rm ext}(Q^2)$ for an external magnetic field are, as mentioned below Eq. (15), suppressed by the separation scale in heavy-quark systems. Therefore, as far as a magnitude of an external field $|e\boldsymbol{B}|$ is small enough to satisfy a hierarchy $|e\boldsymbol{B}| \ll (4m^2 + Q^2)$, we can truncate a series up to dimension-4 operators composed of a product of two field strength tensors $F^{\mu\nu}_{\rm ext} F^{\alpha\beta}_{\rm ext}$. Beyond this separation scale $|e\boldsymbol{B}| \gtrsim (4m^2 + Q^2)$, one has to resum all the terms being proportional to products of an arbitrary number of the field strength tensors. This resummation can be performed by utilizing the proper-time method [77] which has been applied to a vector current correlator (see Ref. [2] for a recent calculation and references therein). Here, we examine effects of magnetic fields in a region $|e\boldsymbol{B}| \lesssim 10 m_\pi^2$ where higher-order terms in $|eB|^n$ are suppressed by $|eB|^n/(4m^2+Q^2)^n \sim (10m_\pi^2)^n/(4m^2+Q^2)^n \ll 1$. Therefore, it is sufficient to include only dimension-4 operators without those higher-dimension operators.

Corrections by the dimension-4 operators are diagrammatically shown in Fig. 4 and have two insertions of external field lines denoted by the wavy lines. Inserted external fields and a one-loop part correspond to an expectation value of the dimension-4 operator and the Wilson coefficient, respectively. We have three diagrams in total. One is a diagram with an insertion on the each quark line (first diagram), and the other two are diagrams with two insertions on either of the quark lines (second diagram). The latter two diagrams provide the same contributions, resulting in a factor of 2.

One of suitable gauges for computation of the diagrams in external fields is the Fock–Schwinger gauge also known as the fixed-point gauge [70,77,78]. Within this gauge, a gauge field for an external constant field is expressed by the field strength tensor $A^\mu_{\rm ext} = x_\nu F^{\nu\mu}_{\rm ext}/2$, and thus a general form of $\Pi^{\rm ext}$ in the OPE (37) is decomposed into the operator part and its coefficient,

$$\Pi^{\rm ext}(q) = C^{\alpha\beta\gamma\delta} \cdot \frac{\alpha_{\rm em}}{\pi} \langle F_{\alpha\beta} F_{\gamma\delta}\rangle, \tag{38}$$

where the Wilson coefficient $C^{\alpha\beta\gamma\delta}$ has Lorentz indices resulting from a trace of the gamma matrices, and the fine structure constant is defined by $\alpha_{\rm em} = e^2/(4\pi) \sim 1/137$. Note again that the correlator $\Pi^{\rm ext}$ and thus $C^{\alpha\beta\gamma\delta}$ are supposed to have additional two Lorentz indices in case of the vector channel, which are suppressed for simplicity.

Calculation for the Wilson coefficient in Eq. (38) can be performed in the same way as that for the dimension-4 (color singlet) gluon condensate $\langle \frac{\alpha_s}{\pi} G^a_{\mu\nu} G^{a\mu\nu}\rangle$ up to a color factor and replacement of the coupling constants. Since the dimension-4 scalar gluon condensate [41,42] and twist-2 gluon condensate [49,53] have been known for some time, we confirm and apply them after taking care of the color factors. To make use of the preceding calculations, it is

useful to decompose the tensor structure in Eq. (38). An antisymmetric property of the field strength tensor leads to decomposition of the right-hand side in Eq. (38) as

$$\Pi^{\rm ext}(q) = \frac{\alpha_{\rm em}}{\pi}[C_0\langle F_{\alpha\beta}F^{\alpha\beta}\rangle + C_2^{\alpha\beta}\langle F_{\alpha\gamma}F_{\beta}{}^{\gamma}\rangle_{\rm TS}], \quad (39)$$

where a subscript "TS" denotes the traceless symmetic part. Parity-odd operators $\langle F_{\alpha\beta}\tilde{F}^{\alpha\beta}\rangle$ and $\langle F_{\alpha\gamma}\tilde{F}_{\beta}{}^{\gamma}\rangle$ would contribute if $C^{\alpha\beta\gamma\delta}$ contained the completely antisymmetric tensor $\epsilon^{\mu\nu\sigma\rho}$. However, this is not the case because $C^{\alpha\beta\gamma\delta}$ is a parity-even quantity containing an even number of $\gamma^5$. The first and second terms would be called scalar and twist-2 terms as in the case of gluon condensates, respectively. While the twist-2 gluon condensate vanishes in the ordinary vacuum because of Lorentz symmetry, we have a nonvanishing contribution of the twist-2 term for external fields in Eq. (39) because externally applied electromagnetic fields break Lorentz symmetry as in the cases of finite temperature and/or density [49,51–53,55,76]. With the decomposed form (39), we can apply preceding calculations of the Wilson coefficients as shown below.

Prior to going into explicit forms of the Wilson coefficients, let us specify a configuration of an external magnetic field. An expectation value of the field strength tensor is given by that of an externally applied classical field,

$$\langle F^{\alpha\beta}\rangle = F^{\alpha\beta}_{\rm ext}. \quad (40)$$

Here, we assume an external magnetic field extending into the positive third direction, of which the field strength tensor is specified by $F^{21}_{\rm ext} = -F^{12}_{\rm ext} = B$ with all the other vanishing elements. In this configuration, an expectation value of the scalar operator in Eq. (39) reads

$$F_0 := \frac{\alpha_{\rm em}}{\pi}\langle F_{\alpha\beta}F^{\alpha\beta}\rangle = \frac{\alpha_{\rm em}}{\pi}\cdot 2B^2. \quad (41)$$

As for the twist-2 operator, we find

$$\frac{\alpha_{\rm em}}{\pi}\langle F^{\alpha\gamma}F^{\beta}{}_{\gamma}\rangle_{\rm TS} = \frac{\alpha_{\rm em}}{\pi}\left(F^{\alpha\gamma}_{\rm ext}F^{\beta}_{{\rm ext}\gamma} - \frac{1}{4}F^{\delta\gamma}_{\rm ext}F^{\rm ext}_{\delta\gamma}g^{\alpha\beta}\right) = F_2(g_{\parallel}^{\alpha\beta} - g_{\perp}^{\alpha\beta}), \quad (42)$$

with an operator expectation value

$$F_2 = \frac{\alpha_{\rm em}}{\pi}\left(-\frac{1}{2}B^2\right). \quad (43)$$

A tensor structure in Eq. (42) is expressed by the metric tensors in the longitudinal and transverse subspaces $g_{\parallel}^{\mu\nu} = {\rm diag}(1,0,0,-1)$ and $g_{\perp}^{\mu\nu} = {\rm diag}(0,-1,-1,0)$, where the directions are meant with respect to the external magnetic field.

Including the external-field part $\Pi^{\rm ext}$ in Eq. (39), we can write down a corresponding part in the moment $M_n = M_n^{\rm vac} + M_n^{\rm ext}$ as

$$M_n^{\rm ext} = A_n(\phi_b^{\rm ext}b_n^{\rm ext} + \phi_c^{\rm ext}c_n^{\rm ext}). \quad (44)$$

The leading-order perturbative part $A_n$ is, as in Eq. (34), extracted as an overall factor, and the first and second terms correspond to the scalar and twist-2 terms. In those terms, the magnetic field strengths are included as

$$\phi_b^{\rm ext} = \kappa\frac{4\pi^2F_0}{9(4m^2)^2} = \frac{Q_c^2}{12}\left(\frac{eB}{m^2}\right)^2, \quad (45)$$

$$\phi_c^{\rm ext} = \kappa\frac{4\pi^2F_2}{3(4m^2)^2} = -\frac{Q_c^2}{16}\left(\frac{eB}{m^2}\right)^2. \quad (46)$$

One should note that the definitions (45) and (46) are the same as those for the scalar and twist-2 gluon condensates (see Eq. (35) and also, e.g., Eqs. (13) and (14) in Ref. [55]), up to a color factor $\kappa = Q_c^2\cdot{\rm Tr}[\mathbf{1}_{\rm color}]/{\rm Tr}[t^at^a] = 6Q_c^2$ with the Gell-Mann matrix $t^a$ normalized to be ${\rm Tr}[t^at^b] = \delta^{ab}/2$ and the electric charge of charm quark $Q_c = 2/3$ in the unit of $|e|$. Since this color factor has been already taken into account in Eqs. (45) and (46), we find a correspondence between the Wilson coefficients for the scalar gluon condensate $\phi_b$ in Eq. (34) and external field $\phi_b^{\rm ext}$ in Eq. (44) to be

$$b_n^{\rm ext} = b_n. \quad (47)$$

Thus, the moment $b_n^{\rm ext}$ for an external magnetic field is the same as that for the scalar gluon condensate $b_n$ summarized in Table 1 in Ref. [42].

We shall proceed to examining the last piece $c_n^{\rm ext}$ from the twist-2 Wilson coefficients. The general forms of the Wilson coefficients for the twist-2 gluon condensate were calculated both in the pseudoscalar and the vector channels [49]. One can apply those expressions to the present cases in external magnetic fields by replacing the expectation value of the operator as

$$\left\langle\frac{\alpha_s}{\pi}G^{\alpha\gamma}G^{\beta}{}_{\gamma}\right\rangle_{\rm TS} \to \kappa\frac{\alpha_{\rm em}}{\pi}\langle F^{\alpha\gamma}F^{\beta}{}_{\gamma}\rangle_{\rm TS}, \quad (48)$$

where the configuration on the right-hand side was specified in Eq. (42). After making the replacement above, one performs the Borel transform.

Below, the twist-2 term $\Pi_2 = C_2^{\alpha\beta}\langle F_{\alpha\gamma}F_{\beta}{}^{\gamma}\rangle_{\rm TS}$ in Eq. (39) will be calculated and then Borel transformed through Eqs. (17) and (19). Those results will be represented by a longitudinal momentum $q_{\parallel}^{\mu} = (q^0,0,0,q^3)$, transverse momentum $q_{\perp}^{\mu} = (0,q^1,q^2,0)$, dimensionless momentum square $\xi = y/4 = Q^2/(4m^2)$, and the Feynman integrals

$$J_n(y) = \int_0^1\frac{1}{\{1+x(1-x)y\}^n}dx. \quad (49)$$

### 1. Pseudoscalar channel

First, we compute the twist-2 Wilson coefficients for the pseudoscalar current (12), of which the general form has been given for the gluon condensate in Eq. (9) in Ref. [49]. Carrying out the replacement (48) in the expression therein, we obtain the twist-2 term in Eq. (39) as

$$\Pi_2^P = \left(\frac{4\pi^2}{3}\right)^{-1} \phi_c^{\rm ext}(q_\parallel^2 - q_\perp^2)\xi^{-2}\chi^P \tag{50}$$

$$\chi^P = \frac{1}{2} + \frac{1}{3}(1-y)J_1 - \frac{1}{6}J_2 - \frac{2}{3}J_3. \tag{51}$$

As mentioned below Eq. (16), we define a dimensionless correlator $\tilde{\Pi}_2 = \Pi_2/q^2$ for the pseudoscalar channel, of which the expression, for a static charmonium carrying a vanishing spatial momentum $q = (\omega, 0, 0, 0)$, is found to be

$$\tilde{\Pi}_2^P = q^{-2}\Pi_2^P = \left(\frac{4\pi^2}{3}\right)^{-1} \phi_c^{\rm ext}\xi^{-2}\chi^P. \tag{52}$$

### 2. Vector channel

Next, we examine the twist-2 term for the vector current (13), of which a general tensor form has been given in Eq. (7) in Ref. [49]. Since the vector current correlator has the two Lorentz indices, we will project them onto the longitudinal and transverse components corresponding to the spin polarization states of a vector meson $J/\psi$. While mass spectra of those spin states are degenerated in cases of static charmonia at finite temperature and/or density, a longitudinal polarization is distinguished from the other two transverse polarizations in external magnetic fields.

Carrying out the replacement (48) in Eq. (7) of Ref. [49] and contracting the Lorentz indices between the operator (42) and the remaining parts, we obtain

$$\Pi_2^{V\mu\nu} = \left(\frac{4\pi^2}{3}\right)^{-1} \phi_c^{\rm ext}\xi^{-2} \times [-2\chi_1^V(P_\parallel^{\mu\nu} - P_\perp^{\mu\nu}) + q^{-2}(q_\parallel^2 - q_\perp^2)\chi_0^V P^{\mu\nu}], \tag{53}$$

where the coefficient functions are given by

$$\chi_0^V = -\frac{2}{3} + 2J_1 - 2J_2 + \frac{2}{3}J_3, \tag{54}$$

$$\chi_1^V = \frac{1}{2} + \left(1 - \frac{1}{3}y\right)J_1 - \frac{3}{2}J_2, \tag{55}$$

and the projection operators are introduced as

$$P^{\mu\nu} = q^2 g^{\mu\nu} - q^\mu q^\nu, \tag{56}$$

$$P_\parallel^{\mu\nu} = q_\parallel^2 g_\parallel^{\mu\nu} - q_\parallel^\mu q_\parallel^\nu, \tag{57}$$

$$P_\perp^{\mu\nu} = q_\perp^2 g_\perp^{\mu\nu} - q_\perp^\mu q_\perp^\nu. \tag{58}$$

The spin polarizations of a vector meson are specified by polarization vectors,

$$\epsilon^\mu = (0, 0, 0, 1), \tag{59}$$

$$\tilde{\epsilon}^\mu = (0, \boldsymbol{n}, 0), \tag{60}$$

where $\boldsymbol{n}$ denotes a unit vector in the transverse plane ($|\boldsymbol{n}| = 1$). We find simple relations $\epsilon_\mu g_\parallel^{\mu\nu} = \epsilon^\nu$, $\tilde{\epsilon}_\mu g_\perp^{\mu\nu} = \tilde{\epsilon}^\nu$ and $\epsilon_\mu g_\perp^{\mu\nu} = \tilde{\epsilon}_\mu g_\parallel^{\mu\nu} = 0$ and some more for a static charmonium carrying $q = (\omega, 0, 0, 0)$ as

$$\epsilon_\mu P^{\mu\nu}\epsilon_\nu = \epsilon_\mu P_\parallel^{\mu\nu}\epsilon_\nu = \tilde{\epsilon}_\mu P^{\mu\nu}\tilde{\epsilon}_\nu = -\omega^2, \tag{61}$$

$$\epsilon_\mu P_\perp^{\mu\nu}\epsilon_\nu = \tilde{\epsilon}_\mu P_\parallel^{\mu\nu}\tilde{\epsilon}_\nu = \tilde{\epsilon}_\mu P_\perp^{\mu\nu}\tilde{\epsilon}_\nu = 0. \tag{62}$$

Therefore, the spin projection of the dimensionless correlator is carried out for the longitudinal polarization as

$$\tilde{\Pi}_2^{V_\parallel} = q^{-2}\cdot\epsilon_\mu(\Pi_2^{V\mu\nu})\epsilon_\nu = \left(\frac{4\pi^2}{3}\right)^{-1}\phi_c^{\rm ext}\xi^{-2}(-\chi_0^V + 2\chi_1^V), \tag{63}$$

and for the transverse polarization as

$$\tilde{\Pi}_2^{V_\perp} = q^{-2}\cdot\tilde{\epsilon}_\mu(\Pi_2^{V\mu\nu})\tilde{\epsilon}_\nu = \left(\frac{4\pi^2}{3}\right)^{-1}\phi_c^{\rm ext}\xi^{-2}(-\chi_0^V). \tag{64}$$

Now that we have the Wilson coefficients obtained in Eqs. (52), (63), and (64), their moments and the simultaneous limits $Q^2, n \to \infty$ can be found straightforwardly. Similarly to the vacuum part (36), the external-field part of the Borel-transformed correlator is found to be[2]

$$\mathcal{M}_{\rm OPE}(\nu) = \pi e^{-\nu}A(\nu)[1 + \alpha_s a(\nu) + (\phi_b + \phi_b^{\rm ext})b(\nu) + \phi_c^{\rm ext}c^{\rm ext}(\nu)], \tag{65}$$

where we have $b^{\rm ext}(\nu) = b(\nu)$ according to Eq. (47), and explicit forms of $c^{\rm ext}(\nu)$ are summarized in Appendix C. The Borel-transformed Wilson coefficients $A(\nu)$, $a(\nu)$, and $b(\nu)$ were obtained in Ref. [72] and are listed in the appendixes in Refs. [55,72]. By using the Borel-transformed OPE (65), we will obtain charmonium spectra in the external magnetic field in the next section.

[2]The vacuum OPE in the vector channel has been performed for a scalar part $\tilde{\Pi}_{\rm vac}^{\rm V}$ in $\Pi_{\rm vac}^{{\rm V},\mu\nu} = (q^\mu q^\nu - q^2 g^{\mu\nu})\tilde{\Pi}_{\rm vac}^{\rm V}$. This result can be applied to the present case, because we need the exactly same quantity $q^{-2}\epsilon_\mu\Pi_{\rm vac}^{{\rm V},\mu\nu}\epsilon_\nu = \tilde{\Pi}_{\rm vac}^{\rm V}$ for a static $J/\psi$ in both the polarization modes specified by the vectors (59) and (60). This normalization is consistent with that on the phenomenological side (22).

## VI. RESULTS AND DISCUSSIONS

In this section, we show charmonium mass spectra obtained from QCD sum rule analyses and then examine roles of magnetically induced mixing terms on the phenomenological side discussed in Sec. IV by comparing the results with those from the hadronic effective theory shown in Sec. II. We also investigate effects of a perturbative heavy-quark loop in an external magnetic field as a subdominant origin of mass modifications.

### A. Mass shifts from QCD sum rules

By means of the exponential sum rule (20), we will investigate charmonium mass spectra by plugging in the phenomenological side elaborated in Sec. IV and all the necessary Wilson coefficients involved in the Borel-transformed correlator (65). Accumulating the OPE (65) and the spectral Ansatz on the phenomenological side shown in Eqs. (29)–(32), the exponential sum rule (20) is expressed as ($\nu = 4m_c^2/M^2$)

$$\mathcal{M}^{J}_{\rm OPE}(\nu) = \mathcal{M}^{J,\rm pole}_{\rm ph}(\nu) + \mathcal{M}^{J,\rm cont}_{\rm ph}(\nu) + \mathcal{M}^{J,\rm ext}_{\rm ph}(\nu). \quad (66)$$

Note that the above expression is for $\eta_c$ and the longitudinal $J/\psi$ ($J = P, V_\parallel$) which have the magnetically induced terms on the phenomenological side. Since the transverse $J/\psi$ does not have those terms, we employ the conventional spectral Ansatz as

$$\mathcal{M}^{\rm V_\perp}_{\rm OPE}(\nu) = \mathcal{M}^{\rm V_\perp,pole}_{\rm ph}(\nu) + \mathcal{M}^{\rm V_\perp,cont}_{\rm ph}(\nu). \quad (67)$$

Inserting these results into the Borel-transformed dispersion relation (66), the mass of the lowest-lying pole can be evaluated from an equation,

$$m^2_{c\bar{c}}(M^2) = -\frac{\partial}{\partial(1/M^2)} \ln[\mathcal{M}_{\rm OPE} - \mathcal{M}^{\rm cont}_{\rm ph} - \mathcal{M}^{\rm ext}_{\rm ph}], \quad (68)$$

where the last term on the rhs, namely the magnetically induced term, is understood to be absent ($\mathcal{M}^{\rm ext}_{\rm ph} = 0$) in the case of the transverse $J/\psi$.

Note that a mass from the QCD sum rule should be independent of a parameter $M^2$ introduced in the Borel transformation. Therefore, one has to examine a stability of the results with respect to variation of $M^2$. Some examples of the $M^2$ dependence of the charmonium masses which are obtained from Eq. (68) and called the Borel curves are shown in Fig. 5. As discussed below Eq. (21), a range of $M^2$ should satisfy two competing conditions for a convergence of the OPE and a pole dominance on the phenomenological side. We require less than 30% contribution from the dimension-4 operators to the OPE and more than 70% lowest-pole dominance in the dispersion integrals (66) and (67), which specifies a Borel window $M^2_{\rm min} < M^2 < M^2_{\rm max}$. The effective threshold parameter $s_0$ is so tuned to make the Borel curve the least sensitive to $M^2$. In the case of charmonia in vacuum, the Borel curve has a minimum $m_{\rm min}$ at $M^2 = M_0^2 > M^2_{\rm min}$ for $s_0 = \infty$ and becomes flatter in $M^2 > M_0^2$ as $s_0$ is decreased. Thus, we evaluate the optimized threshold in $M_0^2 < M^2 < M^2_{\rm max}$ for each value of the magnetic field strength $eB$, giving the $M^2$ dependence of the mass about and less than 10 MeV as seen in Fig. 5. Finally, we average the value of the mass over the same range in the Borel curve and calculate the variance to estimate a systematic error. Details of the systematic framework are described in Ref. [57].

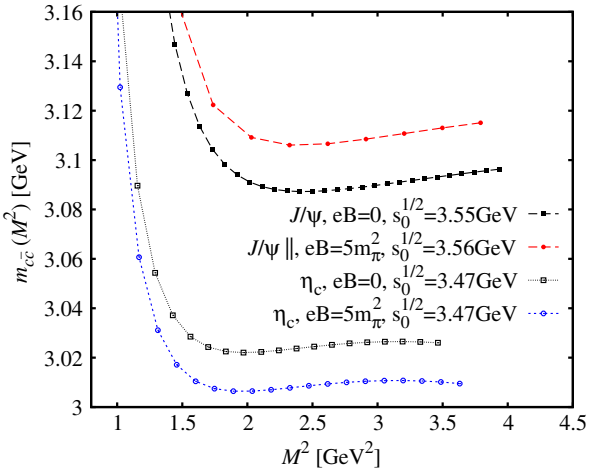


FIG. 5 (color online). Borel curves for $J/\psi$ and $\eta_c$ at $eB = 0$ and $eB = 5m_\pi^2$. $s_0$ is optimized such that $m(M^2)$ is the least sensitive to the variation of $M^2$.

In the QCDSR analyses, we employ parameters $\alpha_s(8m_c^2) = 0.24$, $m_c(p^2 = -2m_c^2) = 1.26\,\text{GeV}$ and $\langle \frac{\alpha_s}{\pi} G^2 \rangle = (0.35\,\text{GeV})^4$ and obtain the vacuum mass of $J/\psi$ and $\eta_c$ to be 3.092 GeV and 3.025 GeV, respectively. To compare results from the QCDSR with those from the effective Lagrangian (3), we insert these vacuum masses into $m_{\rm P,V}$ in Eq. (10). To evaluate the magnetically induced terms on the phenomenological side, we inserted the effective coupling $g_{\rm PV} = 2.095$ obtained in Appendix A which was employed in Eq. (10) as well.

Figure 6 displays the results from the QCDSR. We first focus on $\eta_c$ and the longitudinal $J/\psi$ shown by red and blue curves, respectively. Corresponding Borel curves at $eB = 0$ and $eB = 5m_\pi^2$ are also shown in Fig. 5. To obtain these results, we included the phenomenological side shown on the rhs in Eq. (66) for $\eta_c$ and the longitudinal $J/\psi$, but *not* the double-pole term responsible for the mixing effect in $\mathcal{M}^{\rm ext}_{\rm ph}$ [see Eqs. (31) and (32)]. The role of this term and the appropriate choice of the phenomenological side are discussed below in detail. We compare the results from the QCDSR with those from the hadronic effective theory (10) shown by dashed and dashed-dotted lines. Remarkably, we find a perfect agreement between the results from the two approaches in a relatively weak-field region

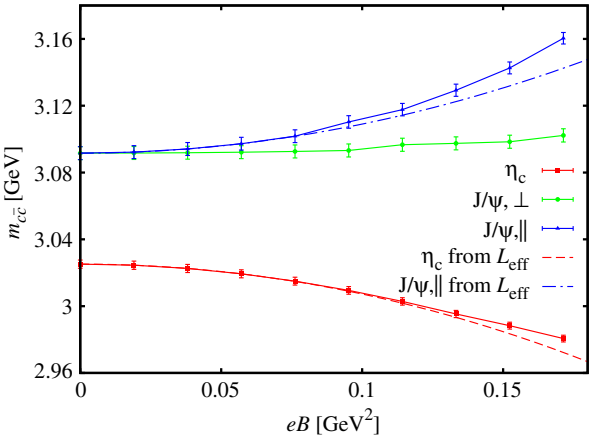


FIG. 6 (color online). Mass of the charmonium states from the QCD sum rules (closed symbols with solid lines) and the effective Langrangian (10) (dashed line for $\eta_c$ and dash-dotted line for $J/\psi$) as functions of $eB$.

$eB < 0.1$ GeV$^2$. This agreement indicates that the magnetically induced terms in Eqs. (31) and (32) are essential ingredients to obtain physically meaningful results in the QCDSR. In this framework, the level repulsion from the mixing effect is simply understood as a consequence of a relative sign of the single-pole terms. In Eq. (31) for $\eta_c$, we have $e^{-m_{\rm V}^2/M^2} - e^{-m_{\rm P}^2/M^2} < 0$ owing to the vacuum mass difference, while the corresponding terms in (32) for the longitudinal $J/\psi$ have an opposite sign, i.e., $e^{-m_{\rm P}^2/M^2} - e^{-m_{\rm V}^2/M^2} > 0$. Therefore, those terms act on masses of $\eta_c$ and the longitudinal $J/\psi$ to shift them in the opposite directions in Eq. (68).

While we obtained a precise agreement in the weak-field region, we find a slight deviation between the results from the QCDSR and the hadronic effective theory as the magnitude of the magnetic field increases. Moreover, we find a slight upward mass shift of the transverse $J/\psi$ shown by a green curve in Fig. 6, although the transverse $J/\psi$ is not mixed with any other lowest-lying charmonium as discussed in Sec. II. Therefore, these deviations would imply some subdominant origins of the mass shifts other than the mixing effect, because the results from the QCDSR contain all the effects implemented in the OPE on the basis of the fundamental degrees of freedom as well as the mixing effect in the hadronic level. In the next section, we will argue that these effects can be separated from the mixing effect with the help of an appropriate choice of the phenomenological side.

### B. Roles of magnetically induced mixing terms on the phenomenological side

In this section, we show QCDSR analyses in two cases by employing (i) the conventional phenomenological side without any magnetically induced term $\mathcal{M}_{\rm ph}^{\rm ext}$ and (ii) a phenomenological side with all the terms in $\mathcal{M}_{\rm ph}^{\rm ext}$ including the double-pole term shown in Eqs. (31) and (32). Comparing those analyses with the one in the last section carried out with the two single poles, we will examine the role of each term in $\mathcal{M}_{\rm ph}^{\rm ext}$. In Figs. 7 and 8, we show results for the $\eta_c$ and longitudinal $J/\psi$ in the cases (i) and (ii) with open symbols and the results in the last section with filled symbols.

First, the red (blue) line denoted as "Single Poles" in Fig. 7 (Fig. 8) reminds us of the results shown in the last section where we included the single pole of the mixing partner $J/\psi$ ($\eta_c$) in addition to the $\eta_c$ ($J/\psi$) pole, without the double pole responsible for the mixing effect discussed below Eq. (28). One should note that, without the double pole on the phenomenological side, all the information of the mass shift encoded in the OPE is reflected in the obtained masses, while, including the double pole, the mixing effect encoded in the OPE will be balanced and canceled by the double-pole term on the phenomenological side. Therefore, the results without the double-pole term

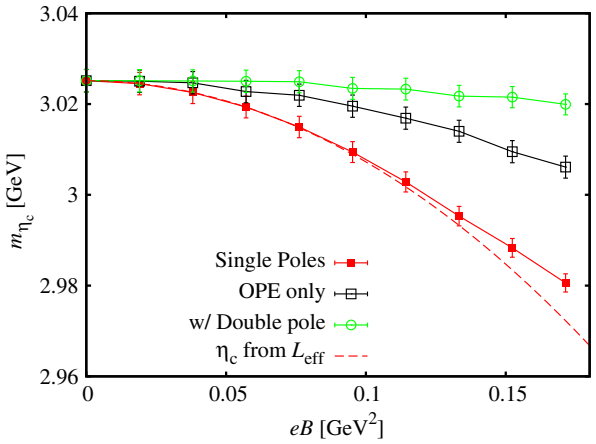


FIG. 7 (color online). Mass of $\eta_c$ from the QCD sum rule with different implementations of the phenomenological side.

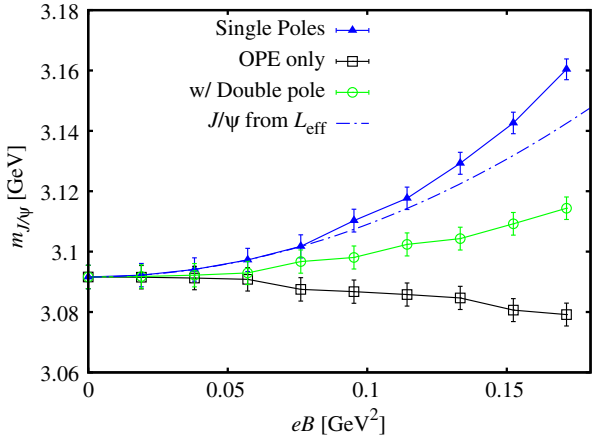


FIG. 8 (color online). Mass of the longitudinal $J/\psi$ from the QCD sum rule with different implementations of the phenomenological side.

show the total mass shifts including the mixing effects as well as other nonperturbative effects from the fundamental degrees of freedom. They are the final results from the QCDSR analysis in the present work.

Second, the black curves include neither the magnetically induced single pole nor the double pole. In this case, obtained mass shifts would be artificial ones, because contributions to the spectral density from both the $\eta_c$ and longitudinal $J/\psi$ poles are attributed to a unique pole assumed as in the conventional QCD sum rules. This leads to an average of the $\eta_c$ and $J/\psi$ masses. Therefore, the mass of $\eta_c$ ($J/\psi$) shown by the black curve deviates from the red (blue) curve toward the mass of the mixing partner $J/\psi$ ($\eta_c$). We conclude that the single pole of the mixing partner has to be included into the spectral Ansatz on the phenomenological side to subtract the contaminating contribution from the mixing partner and to avoid the misleading results due to the averaging.

Finally, the green curves show mass shifts obtained by including all the terms induced by the external magnetic fields. In this analysis, the averaging of masses discussed for the black curves is successfully avoided by including the single pole of the mixing partner, and the mixing effect is subtracted by including the double-pole term which balances the corresponding contributions on the OPE side. Therefore, the green curves show the residual mass shifts caused by nonperturbative effects other than the mixing effect.

The roles of the magnetically induced terms are clear now. On the basis of the above analyses, we conclude that the dominant origin of the mass shifts in the $\eta_c$ and longitudinal $J/\psi$ comes from the mixing between those states as seen in comparison between the sum rule results with implementation of the single poles (red and blue curves) and those from the hadronic effective theory (dashed and dash-dotted lines) and that the residual mass shifts are small in the cases of charmonia. Nevertheless, there are small mass shifts not described by the mixing effect, and the small mass shift in the transverse $J/\psi$ shown in the last section is not involved in the mixing effect. We will then discuss a possible origin of these residual mass shifts in the next section.

### C. Further mixing effects with "continuum"

While we have examined mixing patterns among the charmonium states, any other intermediate state could be contained in the physical spectral density as long as a quantum number is matched. Therefore, as a discussion about possible origins of the residual mass shifts found in the last section, we shall consider interactions between an external magnetic field and a perturbative heavy-quark loop, which are diagrammatically shown in Fig. 9. As in the preceding section, we assume a static charmonium carrying a momentum $q = (2m - \epsilon_0, 0, 0, 0)$ with $\epsilon_0$ being the binding energy. In Fig. 9, a heavy quark and antiquark pair is coupled to the heavy-quark currents with form

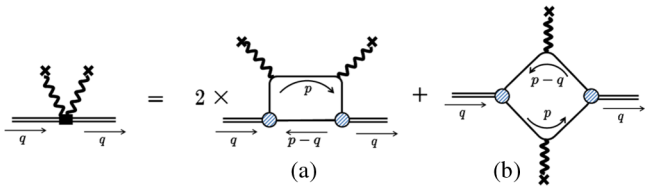


FIG. 9 (color online). A heavy-quark loop as a self-energy of the charmonia in external magnetic fields. Shaded vertices show form factors given by the Bethe–Salpeter amplitudes.

factors given by Bethe–Salpeter amplitudes. The Bethe–Salpeter amplitude was obtained in the ladder approximation and the heavy-quark limit [67] and describes $S$-wave quarkonia in the ordinary vacuum. By using the projection operators

$$P_\pm = \frac{1}{2}(1 \pm \gamma^0), \tag{69}$$

the Bethe–Salpeter amplitudes for $\eta_c$ and $J/\psi$ are, respectively, given by

$$\Gamma^5(p, p-q) = \left(\epsilon_0 + \frac{\boldsymbol{p}^2}{m}\right)\sqrt{\frac{m_{c\bar{c}}}{N_c}}\psi_{1S}(\boldsymbol{p})P_+\gamma^5 P_-, \tag{70}$$

$$\Gamma^\mu(p, p-q) = \left(\epsilon_0 + \frac{\boldsymbol{p}^2}{m}\right)\sqrt{\frac{m_{c\bar{c}}}{N_c}}\psi_{1S}(\boldsymbol{p})P_+\gamma^\mu P_-, \tag{71}$$

where $\psi_{1S}(\boldsymbol{p})$ is a ground-state wave function of the $S$-wave bound state and $m_{c\bar{c}}$ is a mass of $\eta_c$ and $J/\psi$, which is degenerated in the heavy-quark limit. The number of the color degrees of freedom is $N_c = 3$.

We shall evaluate a self-energy of the charmonium caused by an external magnetic field acting on a heavy-quark loop (Fig. 9). Since there are two diagrams (a) and (b) to be taken into account, the self-energy is obtained as a sum of those contributions:

$$-i\Sigma = -2i\Sigma^{(a)} - i\Sigma^{(b)}. \tag{72}$$

By using the quark propagators with insertions of external magnetic fields shown in (B1) and (B2), amplitudes of those diagrams are written down as

$$-i\Sigma^{(a)} = -\int \frac{d^4p}{(2\pi)^4}\,\mathrm{Tr}[\Gamma(p, p-q)S_0(p-q) \times \Gamma^\dagger(p-q, p)S_2(p)], \tag{73}$$

$$-i\Sigma^{(b)} = -\int \frac{d^4p}{(2\pi)^4}\,\mathrm{Tr}[\Gamma(p, p-q)S_1(p-q) \times \Gamma^\dagger(p, p-q)S_1(p)], \tag{74}$$

where $\Gamma$ represents the Bethe–Salpeter amplitude (70) or (71) depending on the channels and $S_0$ is the free

propagator of quarks $S_0(p-q) = i/(\not{p} - \not{q} - m + i\varepsilon)$. In the above expressions, overall minus signs on the right-hand side are associated with a fermion loop, and the QED coupling constants are included in the propagators with external-field insertions.

We computed the amplitudes (73) and (74) in the heavy-quark limit. Following from descriptions in Appendix B 3, we find the self-energies to be

$$\Sigma^5 = \sigma, \tag{75}$$

$$\Sigma^{ij} = \sigma(g_{\parallel}^{ij} - g_{\perp}^{ij}). \tag{76}$$

We obtained a negative scalar quantity $\sigma$ given by

$$\sigma = -\frac{(Q_{\rm em}B)^2}{2m^2}\int\frac{d^3\boldsymbol{p}}{(2\pi)^3}|\psi_{1S}(\boldsymbol{p})|^2\left(2+\frac{4m}{\epsilon_0+\boldsymbol{p}^2/m}\right), \tag{77}$$

which contains a square of the wave function $\psi_{1S}$ and an electric charge $Q_{\rm em} = 2/3|e|$ and mass "$m$" of the quarks interacting with an external magnetic field. We found that the self-energy in the vector channel is finite only in the spatial components $(i,j=1,2,3)$ and that all the others vanish ($\Sigma^{00} = \Sigma^{0i} = \Sigma^{i0} = 0$). Since the metrics in the subspaces distinguish the longitudinal and transverse directions as introduced below (43), we find a mass splitting between the longitudinal and transverse modes of $J/\psi$ in external magnetic fields as shown in a plot below.

Mass shifts of $\eta_c$ and $J/\psi$ due to the self-energies (75) and (76) can be as usual obtained from alternate insertions of the self-energies and the free propagators. Inserting the self-energy $\Sigma^5$ and the free propagator

$$D_0^5(q) = \frac{i}{q^2 - m_{\rm P}^2}, \tag{78}$$

we obtain a resummed propagator,

$$\begin{aligned} D^5(q) &= D_0^5(q) + D_0^5(q)(-i\Sigma^5)D_0^5(q) + \cdots \\ &= \frac{i}{q^2 - m_{\rm P}^2 - \sigma}, \end{aligned} \tag{79}$$

and thus a mass shift of $\eta_c$ to be

$$m_{\rm P}^2(B) = (m_{\rm P}^{\rm vac})^2 + \sigma. \tag{80}$$

As for $J/\psi$, inserting a free propagator in the nonrelativistic limit $(|\boldsymbol{q}| \ll m_{\rm V})$

$$D_0^{ij}(q) = \frac{-i(g^{ij} - q^i q^j/m_{\rm V}^2)}{q^2 - m_{\rm V}^2} \sim \frac{-ig^{ij}}{q^2 - m_{\rm V}^2}, \tag{81}$$

the resummed propagator is obtained as

$$\begin{aligned} D^{ij}(q) &= D_0^{ij}(q) + D_0^{is}(q)(+i\Sigma_{st})D_0^{tj}(q) + \cdots \\ &= \frac{-ig_{\parallel}^{ij}}{q^2 - m_{\rm V}^2 - \sigma} + \frac{-ig_{\perp}^{ij}}{q^2 - m_{\rm V}^2 + \sigma}. \end{aligned} \tag{82}$$

Therefore, we find the polarization-dependent mass shifts given by

$$m_{\rm V\parallel}^2(B) = (m_{\rm V}^{\rm vac})^2 + \sigma \tag{83}$$

$$m_{\rm V\perp}^2(B) = (m_{\rm V}^{\rm vac})^2 - \sigma. \tag{84}$$

To estimate magnitudes of the mass shifts, we evaluate $\sigma$ in Eq. (77) assuming a Coulombic wave function,

$$\psi_{1S}(\boldsymbol{p}) = \frac{8\pi^{1/2}a_0^{3/2}}{((a_0\boldsymbol{p})^2+1)^2}, \tag{85}$$

where the Bohr radius is related to the binding energy as $a_0^2 = (\epsilon_0 m)^{-1}$ and the wave function is normalized as $\int\frac{d^3\boldsymbol{p}}{(2\pi)^3}|\psi_{\rm S}(\boldsymbol{p})|^2 = 1$. Inserting the Coulombic wave function into Eq. (77), the momentum integral is carried out as

$$\int\frac{d^3\boldsymbol{p}}{(2\pi)^3}\left(\frac{4m}{\epsilon_0+\boldsymbol{p}^2/m}\right)|\psi_{1S}(\boldsymbol{p})|^2 = \frac{5}{2}(ma_0)^2, \tag{86}$$

and we obtain the $\sigma$ as a function of the Bohr radius,

$$\sigma = -\frac{(Q_{\rm em}B)^2}{2m^2}\left(2+\frac{5}{2}(ma_0)^2\right). \tag{87}$$

The Bohr radius is related to a mean-square-root radius of a Coulombic bound state as $\langle r^2\rangle = 3a_0^2$, where the mean-square-root radius was estimated as a typical size of the $S$-wave charmonium by fitting the experimental data in terms of the Cornell potential model [73]. Inserting a value $\sqrt{\langle r^2\rangle} = 0.47$ fm obtained in Ref. [73] and the vacuum masses of charmonia into Eqs. (80), (83), and (84), we show the mass shifts due to the self-energies in Fig. 10. Clearly, we find a mass splitting of the longitudinal and transverse $J/\psi$. The heavy-quark loop acts to decrease the longitudinal $J/\psi$ mass, while we have found an increasing longitudinal $J/\psi$ mass in the mixing effect. Varying a value of $\langle r^2\rangle$ as indicated by colored stripes, we confirm that the magnitudes of mass shifts only weakly depend on a value of $\langle r^2\rangle$. To show cooperative effects of the heavy-quark loop and the mixing between $\eta_c$ and the longitudinal $J/\psi$, we replace the vacuum masses in Eqs. (80) and (83) by those from the mixing effects (10). The resultant masses are as precise as the second order in $eB$. In Fig. 11, we find that the mixing effect overwhelms the effect of the heavy-quark loop on the longitudinal $J/\psi$, showing an increasing behavior of the longitudinal $J/\psi$ mass with an increasing $eB$. Comparing Fig. 10 with the results from QCDSR, we find a qualitative agreement in all three of the charmonium

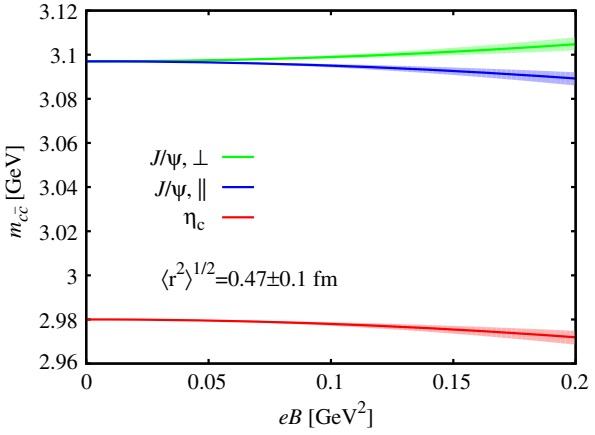


FIG. 10 (color online). Mass shifts of charmonia due to self-energies. Masses of $\eta_c$, longitudinal $J/\psi$, and transverse $J/\psi$ are shown by red, blue, and green curves, respectively. Colored stripes indicate dependences on the sizes of the bound states.

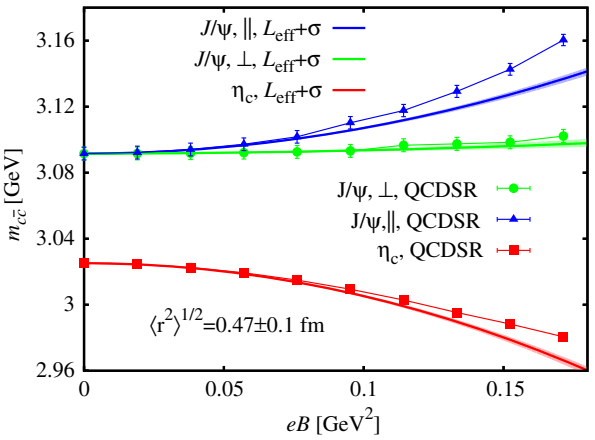


FIG. 11 (color online). Masses from cooperative effects of a heavy-quark loop and a mixing effect, together with the results from QCDSR also shown in Fig. 6. Colors of curves are taken to be the same as in Figs. 6 and 10.

states. The slightly increasing mass of the transverse $J/\psi$ is well reproduced by the heavy-quark loop effect. While we need more detailed information of the physical spectral density to include resonance structures and so on, this agreement implies that the perturbative heavy-quark loop is one of the subdominant origins of the mass shifts in external magnetic fields.

## VII. SUMMARY

We investigated effects of strong magnetic fields on the mass spectra of $S$-wave charmonium states, i.e., $\eta_c$ and $J/\psi$, and elaborated the Ansatz for the spectral density in the QCD sum rule method, the so-called phenomenological side, to consistently manipulate mixing effects in external magnetic fields. We implemented quadratic terms in the order of magnetic fields for the spectral Ansatz and discussed a role of each term on the basis of a partial fraction decomposition (26) and numerical analyses. With an appropriate form of the spectral Ansatz obtained in the present work, we found that the mass shifts of static $\eta_c$ and the longitudinal $J/\psi$ precisely agree with those obtained from an effective Lagrangian approach, indicating that the dominant effect of magnetic fields comes from a level repulsion between those two states. As for the transverse $J/\psi$, we obtained an increasing mass with respect to an increasing magnitude of a magnetic field, while the transverse $J/\psi$ is not mixed with any state.

This behavior of the transverse $J/\psi$ and residual mass shifts of $\eta_c$ and the longitudinal $J/\psi$ imply the existence of some other effects not fully described by the mixing effect in leading-order effective Lagrangian in mesonic degrees of freedom. We examined effects of a mixing effect with higher states and continuum. This was carried out by approximating the intermediate states as a perturbative heavy-quark loop with two insertions of external magnetic fields. We found that this effect gives rise to a splitting between the longitudinal and transverse $J/\psi$ and indeed an increasing mass of the transverse $J/\psi$, while we need more precise information of the spectral density for the higher state and continua to reach a fully conclusive result.

While the residual mass shift, other than the mixing effect, is found to be small for the charmonia, our analysis indicates that one has to take into account effects of the magnetic fields on the phenomenological side consistently to the OPE side. An interesting application would be the QCDSR analysis on light and heavy-light mesons. For instance, a peculiar behavior of the $\rho$ meson spectrum observed in strong magnetic fields by lattice QCD simulations [26,27] might be related to changes of QCD vacuum properties in the strong magnetic field limit as mentioned in the Introduction. As the OPE for such a light meson manifestly includes vacuum expectation values, e.g., a quark condensate $\langle\bar{q}q\rangle$, one could investigate how the vacuum properties are reflected in light-meson spectra by the QCDSR method, where one would expect a larger nonperturbative effect than in charmonia. The elaborate treatment of the mixing effect is necessary even in any other methods involving the spectral density by means of the correlation functions in constant magnetic fields. A general framework discussed in the present work allows for extracting nonperturbative effects of magnetic fields on QCD bound states and will shed light on deeper understanding of the interplay between QCD and QED on the basis of the fundamental degrees of freedom.

## ACKNOWLEDGMENTS

K. H. thanks Hung-chong Kim for fruitful conversations in the early stage of this work. This work was supported by the Korean Research Foundation under Grants No. KRF-2011-0020333 and No. KRF-2011-0030621. K. M. is supported by HIC for FAIR, the Polish Science Foundation

(NCN) under Maestro Grant No. 2013/10/A/ST2/00106 and the Grant-in-Aid for Scientific Research on Innovative Areas from MEXT (Grant No. 24105008). The research of K. H. is supported by JSPS Grants-in-Aid No. 25287066. S. C. was supported in part by the Korean Ministry of Education through the BK21 PLUS program. Three of the authors (K. H., K. M. and S. O.) thank Yukawa Institute for Theoretical Physics, Kyoto University, where a part of this work was discussed during the YIPQS international workshop "*New Frontiers in QCD 2013*."

## APPENDIX A: MIXING STRENGTH FROM EXPERIMENTAL DATA SETS

Here, we determine the coupling constant $g_{\rm PV}$ which gives strength of mixing effects between pseudoscalar and vector mesons. We calculate radiative decay widths in a reaction $J/\psi \to \gamma\eta_c$ by employing the effective vertex (3) and read off the coupling constant by fitting the experimental data.

With the interaction Lagrangian (3), we obtain an invariant amplitude,

$$\begin{aligned}\mathcal{M}_{\rm PV} &= \langle \gamma {\rm P}|\mathcal{L}_{\gamma{\rm PV}}|{\rm V}\rangle \\ &= -\frac{e g_{\rm PV}}{m_0}\epsilon_{\mu\nu\alpha\beta}k_\gamma^\mu \epsilon_\gamma^\nu p_{\rm V}^\alpha \epsilon_{\rm V}^\beta. \end{aligned} \tag{A1}$$

A momentum and polarization vector of the photon (vector meson) are denoted as $k_\gamma^\mu$ and $\epsilon_\gamma^\mu$ ($p_{\rm V}^\mu$ and $\epsilon_{\rm V}^\mu$), respectively. Summing the polarizations of the photon and averaging those of the vector meson, we find

$$\frac{1}{3}\sum_{s_V}\sum_{s_\gamma}|\mathcal{M}_{\rm PV}|^2 = \frac{2}{3}\left(\frac{e g_{\rm PV}}{m_0}\right)^2 m_{\rm V}^2 \tilde{p}^2, \tag{A2}$$

where a magnitude of the center-of-mass momentum in the final state is given by $\tilde{p} = (m_{\rm V}^2 - m_{\rm P}^2)/(2m_{\rm V})$. Integrating over the phase-space volume in the two-body final state, the decay width is then obtained to be

$$\begin{aligned}\Gamma[{\rm V}\to\gamma{\rm P}] &= \frac{\tilde{p}}{8\pi m_{\rm V}^2}\frac{1}{3}\sum_{s_{\rm V}}\sum_{s_\gamma}|\mathcal{M}_{\rm PV}|^2 \\ &= \frac{1}{12}\frac{e^2 g_{\rm PV}^2 \tilde{p}^3}{\pi m_0^2}. \end{aligned} \tag{A3}$$

By fitting the measured radiative decay width, we obtain the coupling constant $g_{\rm PV}$ as

$$g_{\rm PV} = \sqrt{12\pi e^{-2}\tilde{p}^{-3}m_0^2\Gamma_{\rm exp}[{\rm V}\to\gamma{\rm P}]}. \tag{A4}$$

Substituting the measured value $\Gamma_{\rm exp}[J/\psi\to\gamma\eta_c] = 1.579$ keV, we obtain the coupling strength:

$$g_{\rm PV} = 2.095. \tag{A5}$$

## APPENDIX B: MIXING STRENGTHS AND SELF-ENERGY FROM THE BETHE–SALPETER AMPLITUDES

By using the Bethe–Salpeter amplitudes of the $S$-wave quarkonia (70) and (71) obtained in the heavy-quark limit [67], we can also investigate interactions between those quarkonia and external magnetic fields. We provide a calculation of a coupling strength in the mixing between $\eta_c$ and the longitudinal $J/\psi$ from triangle diagrams (Fig. 12), that between the pseudoscalar (vector) current and the longitudinal $J/\psi$ ($\eta_c$) from triangle diagrams shown in Fig. 3, and the self-energies of the quarkonia (Fig. 9). In Appendix B 1, we will find a coupling constant in the mixing between $\eta_c$ and $J/\psi$, of which the simple expression agrees with the one obtained in the leading-order pNRQCD calculation [79] and of which the value is in good agreement with the one obtained by fitting the experimentally measured radiative decay width in Appendix A. In Appendix B 2, we show a mixing strength between a current and a charmonium used for constructing the phenomenological side of the QCD sum rule in Sec. IV. In Appendix B 3, we describe some details in calculation of the self-energy of $\eta_c$ and $J/\psi$ shown in Sec. VI C.

Interactions between quarks and external magnetic fields are taken into account by employing the Fock–Schwinger gauge throughout this section. In this gauge, quark propagators with one and two insertions of constant external fields are expressed as [43]

$$\begin{aligned}S_1(p) &= -\frac{i}{4}Q_{\rm em}F_{\alpha\beta}\frac{1}{(p^2-m^2+i\varepsilon)^2} \\ &\quad\times\{\sigma^{\alpha\beta}(\not{p}+m)+(\not{p}+m)\sigma^{\alpha\beta}\}, \end{aligned} \tag{B1}$$

$$\begin{aligned}S_2(p) &= -\frac{1}{4}Q_{\rm em}^2F_{\alpha\beta}F_{\mu\nu}\frac{1}{(p^2-m^2+i\varepsilon)^5} \\ &\quad\times(\not{p}+m)\{f^{\alpha\beta\mu\nu}+f^{\alpha\mu\beta\nu}+f^{\alpha\mu\nu\beta}\}(\not{p}+m), \end{aligned} \tag{B2}$$

where $Q_{\rm em}$ denotes an electromagnetic charge of a quark and the gamma matrix structures are given by

$$\sigma^{\alpha\beta} = \frac{i}{2}[\gamma^\alpha,\gamma^\beta], \tag{B3}$$

$$f^{\alpha\beta\mu\nu} = \gamma^\alpha(\not{p}+m)\gamma^\beta(\not{p}+m)\gamma^\mu(\not{p}+m)\gamma^\nu. \tag{B4}$$

### 1. Mixing strength between $\eta_c$ and $J/\psi$

We compute the triangle diagrams in Fig. 12 and then read off the effective coupling constant in the mixing between pseudoscalar and vector quarkonia in an external magnetic field. Calculations of the diagrams are performed in the heavy-quark limit, and the final result is found to be independent of the quark mass in the leading order. Also, note that the coupling constant is independent of the wave

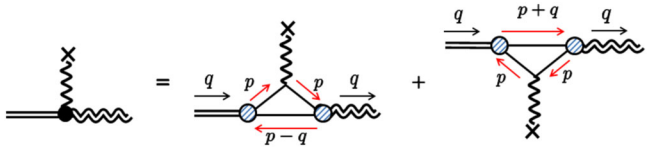


FIG. 12 (color online). An effective coupling strength from triangle diagrams. Shaded vertices show form factors given by the Bethe–Salpeter amplitudes.

functions of charmonia although the Bethe–Salpeter amplitudes contain the wave functions (see Eqs. (70) and (71)).

Let us call the triangle diagrams with clockwise and counterclockwise ordering of vertices diagrams (a) and (b), respectively. We compute a sum of those diagrams

$$i\mathcal{M}^\mu = i\mathcal{M}^\mu_a + i\mathcal{M}^\mu_b, \tag{B5}$$

which are written down as

$$i\mathcal{M}^\mu_a = -\int \frac{d^4p}{(2\pi)^4}\,\mathrm{Tr}[\Gamma^\dagger_5(p-q,p)S_1(p) \times \Gamma^\mu(p,p-q)S_0(p-q)], \tag{B6}$$

$$i\mathcal{M}^\mu_b = -\int \frac{d^4p}{(2\pi)^4}\,\mathrm{Tr}[\Gamma^\dagger_5(p+q,p)S_0(p+q) \times \Gamma^\mu(p,p+q)S_1(p)]. \tag{B7}$$

First, we shall evaluate diagram (a) by carrying out the momentum integral. One of the integrals with respect to the zeroth component can be carried out as a contour integral with a path enclosed either upward or downward in the complex $p^0$ plane. One finds that two poles are enclosed inside the contour in the each case and that one of the two pole contributions is suppressed by an inverse quark mass in the heavy-quark limit. Enclosing the contour upward for a simplicity of the calculation, we pick up the leading contribution from the pole located on

$$\bar{p}^0_a = q^0 - \epsilon_{\boldsymbol{p}-\boldsymbol{q}} \simeq m - \left(\epsilon_0 + \frac{\boldsymbol{p}^2}{2m}\right), \tag{B8}$$

where $\epsilon_0$ is a binding energy as mentioned in the beginning of Sec. VI C and the approximate equality is valid in the heavy-quark limit. At this pole, we have a residue obtained from the limiting values,

$$\lim_{p^0\to\bar{p}^0_a}(p^0 - p^0_a)S_0(p-q) \sim -P_-, \tag{B9}$$

$$\lim_{p^0\to\bar{p}^0_a} S_1(p) \sim -\frac{i}{4}Q_{\mathrm{em}}F_{\alpha\beta}\frac{\sigma^{\alpha\beta}P_+ + P_+\sigma^{\alpha\beta}}{2m(\epsilon_0 + \boldsymbol{p}^2/m)^2}, \tag{B10}$$

and thus the integral in diagram (a) is evaluated as

$$i\mathcal{M}^\mu_a = 2Q_{\mathrm{em}}\tilde{F}^{0\mu}\int\frac{d^3\boldsymbol{p}}{(2\pi)^3}|\psi_{1S}(\boldsymbol{p})|^2. \tag{B11}$$

Similarly, we evaluate diagram (b) by maintaining the leading pole contribution with the contour enclosed downward. Picking up the pole at

$$\bar{p}^0_b = -q^0 + \epsilon_{\boldsymbol{p}-\boldsymbol{q}} \simeq -m + \left(\epsilon_0 + \frac{\boldsymbol{p}^2}{2m}\right), \tag{B12}$$

we have

$$\lim_{p^0\to\bar{p}^0_b}(p^0 - p^0_b)S_0(p+q) \sim P_+ \tag{B13}$$

$$\lim_{p^0\to\bar{p}^0_b} S_1(p) \sim -\frac{i}{4}Q_{\mathrm{em}}F_{\alpha\beta}\frac{\sigma^{\alpha\beta}P_- + P_-\sigma^{\alpha\beta}}{2m(\epsilon_0 + \boldsymbol{p}^2/m)^2} \tag{B14}$$

and then find that diagram (b) provides the same contribution as that of diagram (a),

$$i\mathcal{M}^\mu_b = i\mathcal{M}^\mu_a. \tag{B15}$$

Therefore, we obtain the sum of two triangle diagrams as

$$\begin{aligned} i\mathcal{M}^\mu &= 2\times 2Q_{\mathrm{em}}\tilde{F}^{0\mu}\int\frac{d^3\boldsymbol{p}}{(2\pi)^3}|\psi_{1S}(\boldsymbol{p})|^2 \\ &= 4Q_{\mathrm{em}}\tilde{F}^{0\mu}. \end{aligned} \tag{B16}$$

Note that the second line follows from a normalization of the wave function

$$\int\frac{d^3\boldsymbol{p}}{(2\pi)^3}|\psi_{1S}(\boldsymbol{p})|^2 = 1, \tag{B17}$$

and thus the amplitude is independent of the wave functions. We obtain the mixing amplitude between the pseudoscalar and the longitudinal (transverse) mode of the vector state by contracting with the polarization vector $\epsilon^\mu$ ($\tilde{\epsilon}^\mu$) [see Eqs. (59) and (60)]. When an external magnetic field is applied in the positive third direction ($\tilde{F}^{30} = -\tilde{F}^{03} = B$), we find an amplitude for the longitudinal mode as

$$i\mathcal{M}_\mu\epsilon^\mu = 4Q_{\mathrm{em}}\tilde{F}^{0\mu}\epsilon_\mu = 4Q_{\mathrm{em}}B, \tag{B18}$$

while an amplitude for the transverse modes vanishes,

$$i\mathcal{M}_\mu\tilde{\epsilon}^\mu = 0. \tag{B19}$$

As a wrap up, we found that only the longitudinal mode of the vector state can mix with the pseudoscalar state in an external magnetic field and that an effective vertex of the interaction among a photon, the pseudoscalar state, and the longitudinal mode of the vector state is given by

$$\mathcal{L}_{\gamma \mathrm{PV}} = \frac{4Q_{\mathrm{em}}}{m_0} \tilde{F}_{\mu\nu} (\partial^\mu P) V^\nu. \tag{B20}$$

The coupling constant depends only on an electric charge of a heavy quark and is given by $g_{\mathrm{PV}} = 8/3 \simeq 2.66$ ($g_{\mathrm{PV}} = 4/3 \simeq 1.33$) for the transition between $\eta_c$ and $J/\psi$ ($\eta_b$ and $\Upsilon$). This is consistent with the value obtained by fitting the measured radiative decay width (A5), but slightly overestimated. We also note that we can calculate the radiative decay widths in $J/\psi \to \eta_c + \gamma$ and $\Upsilon \to \eta_b + \gamma$ by using an effective vertex (B20), resulting in expressions consistent with those from the leading-order calculation by pNRQCD [79]. The overestimate mentioned above was improved, owing to subleading terms in pNRQCD [79].

### 2. Direct-mixing strength

We compute the direct-coupling strength between the heavy-quark current and charmonium depicted in Fig. 3. Amplitudes of theses two diagrams are written down similarly to Eqs. (B6) and (B7) as

$$i\mathcal{M}_a^\mu = -\int \frac{d^4p}{(2\pi)^4} \mathrm{Tr}[i\gamma^5 S_1(p) \times \Gamma^\mu(p, p-q) S_0(p-q)], \tag{B21}$$

$$i\mathcal{M}_b^\mu = -\int \frac{d^4p}{(2\pi)^4} \mathrm{Tr}[i\gamma^5 S_0(p+q) \times \Gamma^\mu(p, p+q) S_1(p)]. \tag{B22}$$

We evaluate the energy integrals in the above as in the calculation in Appendix B 1 and obtain

$$i\mathcal{M}_a^\mu = i\mathcal{M}_b^\mu = -iQ_{\mathrm{em}} \frac{\sqrt{N_c m_{c\bar{c}}}}{2m} \tilde{F}^{0\mu} \int \frac{d^3\boldsymbol{p}}{(2\pi)^3} \frac{\psi_{1S}(\boldsymbol{p})}{\epsilon_0 + \boldsymbol{p}^2/m}. \tag{B23}$$

We find that only the longitudinal $J/\psi$ having a polarization vector $\epsilon^\mu$ is directly created from the pseudoscalar current in the presence of external magnetic fields, since the above amplitude is proportional to $\tilde{F}^{0\mu}$. Assuming a Coulombic wave function (85) for $J/\psi$, we find the direct-coupling strength as

$$f_{\mathrm{dir}} = \left| -2iQ_{\mathrm{em}} \frac{\sqrt{N_c m_{c\bar{c}}}}{2m} \frac{\tilde{F}^{0\mu}\epsilon_\mu}{4\pi^{1/2} a_0^{3/2} \epsilon_0^{1/2}} \right|^2 = f \frac{a_0^4 (Q_{\mathrm{em}} B)^2}{64}, \tag{B24}$$

where $f$ is a coupling strength between the heavy-quark currents and the charmonia in the ordinary vacuum without external magnetic fields. This strength follows from the square of an amplitude,

$$i\mathcal{M} = -\int \frac{d^4p}{(2\pi)^4} \mathrm{Tr}[\gamma S_0(p) \Gamma(p, p-q) S_0(p-q)], \tag{B25}$$

with $\gamma$ and $\Gamma$ meaning $i\gamma^5$ and $\Gamma^5$ ($\gamma^\mu$ and $\Gamma^\mu$) appearing in a coupling between the pseudoscalar (vector) current and $\eta_c$ ($J/\psi$). By performing the integrals as in the above computations, we find in both channels

$$f = \frac{4m_{c\bar{c}} N_c}{\pi a_0^3}. \tag{B26}$$

### 3. Heavy-quark loop

We evaluate the self-energy of charmonia in an magnetic field shown in Fig. 9. Diagrammatic calculation is performed in the heavy-quark limit and thus proceeds in a similar way to the calculation in the previous sections.

We shall first examine diagram (a) in Fig. 9, the amplitude of which is written down in Eq. (73). We carry out an integral with respect to the zeroth component of a loop momentum $p$ with a contour enclosed upward. We pick up the leading contribution from a pole located on

$$\bar{p}^0 = q^0 - \epsilon_{\boldsymbol{p}-\boldsymbol{q}} \simeq m - \epsilon_0 - \frac{\boldsymbol{p}^2}{2m}, \tag{B27}$$

providing a residue given by

$$\mathrm{Res}_{p^0=\bar{p}^0}[\Gamma(p, p-q) S_0(p-q) \Gamma^\dagger(p-q, p) S_2(p)] = [\Gamma(p, p-q)(-P_-) \Gamma^\dagger(p-q, p)(\lim_{p^0 \to \bar{p}^0} S_2(p))], \tag{B28}$$

where we use the projection operators (69) which have properties utilized below, $P_\pm P_\mp = 0$, $P_\pm^2 = P_\pm$ and $\gamma^0 P_\pm = P_\pm \gamma^0 = \pm P_\pm$. A limiting expression of the quark propagator with two insertions is given by

$$\lim_{p^0 \to \bar{p}^0} S_2(p) \sim \frac{1}{4} Q_{\mathrm{em}}^2 F_{\alpha\beta} F_{\mu\nu} \frac{1}{(\epsilon_0 + \boldsymbol{p}^2/m)^5} \times P_+ \{f'_{\alpha\beta\mu\nu} + f'_{\alpha\mu\beta\nu} + f'_{\alpha\mu\nu\beta}\} P_+ \tag{B29}$$

with $f'^{\alpha\beta\mu\nu} = \gamma^\alpha P_+ \gamma^\beta P_+ \gamma^\mu P_+ \gamma^\nu$. Commuting the gamma matrices as $\gamma^\alpha P_+ = g^{0\alpha} + P_- \gamma^\alpha$, we find

$$P_+ f'^{\alpha\beta\mu\nu} P_+ = g^{0\alpha} g^{0\beta} g^{0\mu} g^{0\nu} P_+, \tag{B30}$$

and thus that the amplitude $\Sigma^{(a)}$ is proportional to the vanishing (0,0) component of the field strength tensors. Therefore, the contribution from diagram (a) vanishes in the leading order in the heavy-quark limit, so we have found in both pseudoscalar and vector states

$$\Sigma^{(a)} \sim 0, \tag{B31}$$

and thus $\Sigma \sim \Sigma^{(b)}$.

We shall proceed to examining diagram (b), the amplitude of which is written down in Eq. (74). As in the calculation of diagram (a), we enclose a contour downward and pick up a residue at the same pole (B27). One would, however, have to compute a residue at a double pole, because the quark propagator with an insertion $S_1(p-q)$ has a double-pole structure. The residue is thus obtained by operating a derivative as

$$\begin{aligned}&\mathrm{Res}_{p^0=\bar{p}^0}[\Gamma(p,p-q)S_1(p-q)\Gamma^\dagger(p-q,p)S_1(p)]\\&=\lim_{p^0\to\bar{p}^0}\left[\Gamma(p,p-q)\mathcal{S}(p-q)\Gamma^\dagger(p-q,p)\frac{d}{dp^0}S_1(p)\right.\\&\left.+\Gamma(p,p-q)\left(\frac{d}{dp^0}\mathcal{S}(p-q)\right)\Gamma^\dagger(p-q,p)S_1(p)\right],\end{aligned} \tag{B32}$$

where a shorthand notation is introduced as $\mathcal{S}(p-q) = (p^0-\bar{p}^0)^2 S_1(p-q)$. Some ingredients necessary for obtaining the residue follow from operation of the limits and derivatives, for the first term in Eq. (B32), as

$$\begin{aligned}\lim_{p^0\to\bar{p}^0}\frac{d}{dp^0}S_1(p) &= -\frac{i}{4}Q_{\mathrm{em}}F_{\alpha\beta}\frac{1}{(2m)^2(\epsilon_0+\boldsymbol{p}^2/m)^3}\\&\times[(\epsilon_0+\boldsymbol{p}^2/m)(\sigma^{\alpha\beta}\gamma^0+\gamma^0\sigma^{\alpha\beta})\\&+4m(\sigma^{\alpha\beta}P_+ + P_+\sigma^{\alpha\beta})]\end{aligned} \tag{B33}$$

$$\lim_{p^0\to\bar{p}^0}\mathcal{S}(p-q) = -\frac{i}{4}Q_{\mathrm{em}}F_{\alpha\beta}\frac{1}{2m}\{\sigma^{\alpha\beta}P_- + P_-\sigma^{\alpha\beta}\} \tag{B34}$$

and, for the second term, as

$$\begin{aligned}\lim_{p^0\to\bar{p}^0}\frac{d}{dp^0}\mathcal{S}(p-q) &= -\frac{i}{4}Q_{\mathrm{em}}F_{\alpha\beta}\frac{1}{(2m)^2}\\&\times[\sigma^{\alpha\beta}(\gamma^0+2P_-)+(\gamma^0+2P_-)\sigma^{\alpha\beta}]\end{aligned} \tag{B35}$$

$$\lim_{p^0\to\bar{p}^0}S_1(p) \sim -\frac{i}{4}Q_{\mathrm{em}}F_{\alpha\beta}\frac{\{\sigma^{\alpha\beta}P_+ + P_+\sigma^{\alpha\beta}\}}{2m(\epsilon_0+\frac{\boldsymbol{p}^2}{m})^2}. \tag{B36}$$

Substituting the limiting behaviors of the propagators (B33) and (B36) into Eq. (B32), we find a self-energy of $\eta_c$ as

$$\begin{aligned}-i\Sigma^{(b)} &= i\frac{Q_{\mathrm{em}}^2}{16m^2}F_{\mu\nu}F_{\alpha\beta}\mathrm{Tr}[P_-\sigma^{\mu\nu}P_-\sigma^{\alpha\beta}]\\&\times\int\frac{d^3\boldsymbol{p}}{(2\pi)^3}|\psi_{1S}(\boldsymbol{p})|^2\left(2+\frac{4m}{(\epsilon_0+\boldsymbol{p}^2/m)}\right)\end{aligned} \tag{B37}$$

and a self-energy of $J/\psi$ as

$$\begin{aligned}-i\Sigma^{(b)\lambda\sigma} &= i\frac{Q_{\mathrm{em}}^2}{16m^2}F^{\mu\nu}F^{\alpha\beta}\Phi^{\lambda\sigma}_{\mu\nu\alpha\beta}\\&\times\int\frac{d^3\boldsymbol{p}}{(2\pi)^3}|\psi_{1S}(\boldsymbol{p})|^2\left(2+\frac{4m}{(\epsilon_0+\boldsymbol{p}^2/m)}\right).\end{aligned} \tag{B38}$$

A trace of the gamma matrices is given by $\Phi^{\lambda\sigma}_{\mu\nu\alpha\beta} = \mathrm{Tr}[(P_+\gamma^\lambda P_-)\sigma_{\mu\nu}(P_-\gamma^\sigma P_+)\sigma_{\alpha\beta}]$. Carrying out the traces, we obtain the self-energies (75) and (76) for $\eta_c$ and $J/\psi$, respectively. External magnetic fields do not give rise to a self-energy of the unphysical mode of $J/\psi$, since the Bethe–Salpeter amplitude vanishes for a temporal mode $(\lambda,\sigma=0)$ when the charmonium is at rest.

We comment on the second-order Stark effect caused by external electric fields [80–82]. This term can be obtained by including the higher-dimensional operator correction to the Bethe–Salpeter equation in (70) and (71) that is proportional to the external electric field operator and the wave function (see the second paper in Ref. [67]). The effective four-point vertex between the charmonium, external field, charm, and anticharm is given as [67]

$$M_4^{\nu\mu} = ig\sqrt{\frac{m_{c\bar{c}}}{N_c}}\left(\frac{\partial\psi_{1S}}{\partial p^\alpha}\right)F_E^{\nu\alpha}P_+\Gamma_\mu P_-, \tag{B39}$$

where $\Gamma_\mu$ is $\gamma_\mu$ or $i\gamma^5$ for $J/\psi$ or $\eta_c$, respectively. Also, the subscript $E$ in the field strength tensor means that only the electric part of the field strength tensor is taken. Substituting this into the $J/\psi$ self-energy,

$$\begin{aligned}\Sigma &= -i\int\frac{d^4p}{(2\pi)^4}\,\mathrm{Tr}[M_4^{0\mu}S_0(p-q)M_4^{\dagger 0}{}_\mu S_0(p)]\\&= -\frac{2m_{\mathrm{V}}}{18}\int_0^\infty dp^2\left|\frac{\partial\psi_{1S}}{\partial p}\right|^2\frac{p}{\epsilon+p^2/m}\left\langle\frac{\alpha}{\pi}E^2\right\rangle,\end{aligned} \tag{B40}$$

which gives the second-order Stark effect formula for the external gauge field [54]. The same formula is obtained for $\eta_c$.

It has been found that the leading-order effect on charmonia by external fields is due to external electric field and that effects of magnetic field are subleading in the heavy-quark expansion [82]. We find that the self-energies in magnetic fields (B37)–(B38) are also suppressed by a factor of $1/m^2$ compared to the second-order Stark effect formula (B40). Inserting a field strength tensor of an electric field given by temporal components, $F^{0i} = -F^{i0} = E^i$, the trace parts in Eqs. (B37) and (B38) identically vanish when any of the Lorentz indices, $\alpha$, $\beta$, $\mu$, or $\nu$, takes temporal component because of simple

identities $P_\pm\sigma^{0i}P_\pm = \sigma^{0i}P_\mp P_\pm = 0$, showing that there is no additional term contributing to the second-order Stark effect formula.

## APPENDIX C: BOREL-TRANSFORMED WILSON COEFFICIENTS

In this Appendix, we provide a table of the twist-2 Wilson coefficients $c_n^{\rm ext}$ and $c^{\rm ext}(\nu)$ which are obtained by carrying out the Borel transform of $\tilde{\Pi}_2$ shown in Sec. V B.

The moments $c_n^{\rm ext}$ are typically represented by the Gauss hypergeometric function ${}_2F_1(a,b,c;\rho)$ which is, in conventions in Refs. [41,42], defined by

$$ {}_2F_1(a,b,c;\rho) = \frac{1}{B(a,c-a)} \times \int_0^1 dt t^{a-1}(1-t)^{c-a-1}(1-\rho t)^{-b}, \quad \text{(C1)} $$

where the beta function $B(x,y)$ is related to the gamma function as $B(x,y) = \Gamma(x)\cdot\Gamma(y)/\Gamma(x+y)$. Hereafter, we suppress the subscripts as $F(a,b,c;\rho) = {}_2F_1(a,b,c;\rho)$ for simplicity. Following from the definition of the Borel transform (17), we obtained a useful formula,

$$ \begin{aligned} &\frac{(-1)^n}{n!}\frac{d^n}{d\xi^n}(\xi^{-\beta}J_k(\xi)) \\ &= \frac{(-1)^\beta\sqrt{\pi}}{2}\frac{\Gamma(n+k+\beta)}{\Gamma(k)\Gamma(n+\beta+\frac{3}{2})} \\ &\quad\times(1-\rho)^{n+1}F\left(n+1,\frac{3}{2}-k,n+\beta+\frac{3}{2};\rho\right), \end{aligned} \quad \text{(C2)} $$

for general integers $\beta$ and $k$. Relevant variables are

$$ \xi = \frac{Q^2}{4m^2}, \quad \text{(C3)} $$

$$ \rho = \frac{\xi}{1+\xi}, \quad \text{(C4)} $$

$$ \nu = \frac{4m^2}{M^2} = n(1-\rho), \quad \text{(C5)} $$

and the Borel mass $M^2 = Q^2/n$ is maintained being a constant in the infinite limits (19). In these limits, the Whittaker function

$$ G(b,c;\nu) = \frac{1}{\Gamma(c)}\int_0^\infty e^{-t}t^{c-1}(\nu+t)^{-b}dt \quad \text{(C6)} $$

is related to a limiting behavior of the hypergeometric function as

$$ F(b,\ell,\ell+c;\rho) \underset{[n\to\infty]}{\to} \ell^b G(b,c;\nu), \quad \text{(C7)} $$

so that the Borel-transformed Wilson coefficients $c^{\rm ext}(\nu)$ can be obtained analytically and represented by the Whittaker function [72]. The Wilson coefficients $b_n$ and $b(\nu)$ appearing below are shown in Ref. [42] and Refs. [55,72], respectively.

### 1. Pseudoscalar channel (P)

$$ c_n^{\rm P,ext} = \frac{4}{3}\left[b_n - 4n(n+1)(1-\rho)\frac{F(n+1,-\frac{1}{2},n+\frac{3}{2};\rho)}{F(n,\frac{1}{2},n+\frac{3}{2};\rho)}\right] \quad \text{(C8)} $$

$$ \begin{aligned} c^{\rm P,ext}(\nu) = \frac{\nu}{2G(\frac{1}{2},\frac{3}{2};\nu)}\Bigg[&-G\left(-\frac{3}{2},\frac{3}{2};\nu\right) \\ &+6G\left(-\frac{1}{2},\frac{3}{2};\nu\right) - 8G\left(-\frac{1}{2},\frac{1}{2};\nu\right)\Bigg] \end{aligned} \quad \text{(C9)} $$

### 2. Vector channel (V)

#### a. Longitudinal mode ($\mathrm{V}_\parallel$)

$$ \begin{aligned} c_n^{\mathrm{V}_\parallel,\rm ext} = &\frac{4n(n+2)(1-\rho)}{3(2n+5)F(n,\frac{1}{2},n+\frac{5}{2};\rho)} \\ &\times\Bigg[\frac{4}{n+2}F\left(n+1,\frac{1}{2},n+\frac{5}{2};\rho\right) \\ &-3(n+3)(n+4)F\left(n+1,-\frac{1}{2},n+\frac{7}{2};\rho\right) \\ &-(n+3)(n+4)F\left(n+1,-\frac{3}{2},n+\frac{7}{2};\rho\right)\Bigg] \end{aligned} \quad \text{(C10)} $$

$$ \begin{aligned} c^{\mathrm{V}_\parallel,\rm ext}(\nu) = \frac{2\nu}{3G(\frac{1}{2},\frac{5}{2};\nu)}\Bigg[&8G\left(\frac{1}{2},\frac{3}{2};\nu\right) - 3G\left(-\frac{1}{2},\frac{5}{2};\nu\right) \\ &- G\left(-\frac{3}{2},\frac{5}{2};\nu\right)\Bigg] \end{aligned} \quad \text{(C11)} $$

#### b. Transverse mode ($\mathrm{V}_\perp$)

$$ \begin{aligned} c_n^{\mathrm{V}_\perp,\rm ext} = &\frac{4n(n+2)(1-\rho)}{3(2n+5)F(n,\frac{1}{2},n+\frac{5}{2};\rho)} \\ &\times\Bigg[6F\left(n+1,\frac{1}{2},n+\frac{7}{2};\rho\right) \\ &+6(n+3)F\left(n+1,-\frac{1}{2},n+\frac{7}{2};\rho\right) \\ &-(n+3)(n+4)F\left(n+1,-\frac{3}{2},n+\frac{7}{2};\rho\right)\Bigg] \end{aligned} \quad \text{(C12)} $$

$$ \begin{aligned} c^{\mathrm{V}_\perp,\rm ext}(\nu) = \frac{2\nu}{3G(\frac{1}{2},\frac{5}{2};\nu)}\Bigg[&6G\left(\frac{1}{2},\frac{5}{2};\nu\right) \\ &+6G\left(-\frac{1}{2},\frac{5}{2};\nu\right) - G\left(-\frac{3}{2},\frac{5}{2};\nu\right)\Bigg] \end{aligned} \quad \text{(C13)} $$

[1] W. Heisenberg and H. Euler, Z. Phys. **98**, 714 (1936), arXiv: physics/0605038; W. Dittrich and M. Reuter, Lect. Notes Phys. **220**, 1 (1985); W. Dittrich and H. Gies, Springer Tracts Mod. Phys. **166**, 1 (2000); G. V. Dunne, *From Fields to Strings: Circumnavigating Theoretical Physics*, Vol. I (World Scientific, Singapore, 2005).

[2] For recent calculations, e.g., K. Hattori and K. Itakura, Ann. Phys. **330**, 23 (2013); **334**, 58 (2013).

[3] R. C. Duncan and C. Thompson, Astrophys. J. Lett. **392**, L9 (1992); C. Thompson and R. C. Duncan, Mon. Not. R. Astron. Soc. **275**, 255 (1995); Astrophys. J. **473**, 322 (1996).

[4] A. K. Harding and D. Lai, Rep. Prog. Phys. **69**, 2631 (2006).

[5] S. Schramm, B. Muller, and A. J. Schramm, Mod. Phys. Lett. A **07**, 973 (1992); Phys. Lett. A **164**, 28 (1992).

[6] D. E. Kharzeev, L. D. McLerran, and H. J. Warringa, Nucl. Phys. **A803**, 227 (2008); K. Fukushima, D. E. Kharzeev, and H. J. Warringa, Phys. Rev. D **78**, 074033 (2008); H. J. Warringa, Phys. Rev. D **86**, 085029 (2012).

[7] V. Skokov, A. Y. Illarionov, and V. Toneev, Int. J. Mod. Phys. A **24**, 5925 (2009); V. Voronyuk, V. D. Toneev, W. Cassing, E. L. Bratkovskaya, V. P. Konchakovski, and S. A. Voloshin, Phys. Rev. C **83**, 054911 (2011); A. Bzdak and V. Skokov, Phys. Lett. B **710**, 171 (2012); W. T. Deng and X. G. Huang, Phys. Rev. C **85**, 044907 (2012).

[8] K. Itakura, in *Proceedings of the International Conference on Physics in Intense Fields (PIF2010)*, edited by K. Itakura *et al.* (KEK, Tsukuba, 2011), http://ccdb5fs.kek.jp/tiff/2010/1025/1025013.pdf.

[9] B. L. Ioffe and A. V. Smilga, Nucl. Phys. **B232**, 109 (1984).

[10] S. P. Klevansky and R. H. Lemmer, Phys. Rev. D **39**, 3478 (1989); S. P. Klevansky, J. Janicke, and R. H. Lemmer, Phys. Rev. D **43**, 3040 (1991); H. Suganuma and T. Tatsumi, Ann. Phys. **208**, 470 (1991); S. P. Klevansky, Rev. Mod. Phys. **64**, 649 (1992).

[11] V. P. Gusynin, V. A. Miransky, and I. A. Shovkovy, Phys. Rev. Lett. **73**, 3499 (1994); Phys. Rev. D **52**, 4718 (1995); **52**, 4747 (1995); Phys. Lett. B **349**, 477 (1995); Nucl. Phys. **B462**, 249 (1996).

[12] D. K. Hong, Y. Kim, and S.-J. Sin, Phys. Rev. D **54**, 7879 (1996); D. K. Hong, Phys. Rev. D **57**, 3759 (1998); G. W. Semenoff, I. A. Shovkovy, and L. C. R. Wijewardhana, Phys. Rev. D **60**, 105024 (1999).

[13] I. A. Shushpanov and A. V. Smilga, Phys. Lett. B **402**, 351 (1997); N. O. Agasian and I. A. Shushpanov, Phys. Lett. B **472**, 143 (2000); T. D. Cohen, D. A. McGady, and E. S. Werbos, Phys. Rev. C **76**, 055201 (2007).

[14] C. N. Leung, Y. J. Ng, and A. W. Ackley, Phys. Rev. D **54**, 4181 (1996); D. S. Lee, C. N. Leung, and Y. J. Ng, Phys. Rev. D **55**, 6504 (1997); E. J. Ferrer and V. de la Incera, Phys. Lett. B **481**, 287 (2000); D. Kabat, K. Lee, and E. Weinberg, Phys. Rev. D **66**, 014004 (2002); A. Ayala, A. Bashir, A. Raya, and E. Rojas, Phys. Rev. D **73**, 105009 (2006); E. Rojas, A. Ayala, A. Bashir, and A. Raya, Phys. Rev. D **77**, 093004 (2008).

[15] P. V. Buividovich, M. N. Chernodub, E. V. Luschevskaya, and M. I. Polikarpov, Phys. Lett. B **682**, 484 (2010); M. DfElia and F. Negro, Phys. Rev. D **83**, 114028 (2011).

[16] G. S. Bali, F. Bruckmann, G. Endrődi, Z. Fodor, S. D. Katz, S. Krieg, A. Schäfer, and K. K. Szabó, J. High Energy Phys. 02 (2012) 044; G. S. Bali, F. Bruckmann, G. Endrődi, Z. Fodor, S. D. Katz, and A. Schäfer, Phys. Rev. D **86**, 071502 (2012).

[17] P. V. Buividovich, M. N. Chernodub, E. V. Luschevskaya, and M. I. Polikarpov, Nucl. Phys. **B826**, 313 (2010); G. S. Bali, F. Bruckmann, M. Constantinou, M. Costa, G. Endrődi, S. D. Katz, H. Panagopoulos, and A. Schäfer, Phys. Rev. D **86**, 094512 (2012); M. D'Elia, M. Mariti, and F. Negro, Phys. Rev. Lett. **110**, 082002 (2013); C. Bonati, M. D'Elia, M. Mariti, F. Negro, and F. Sanfilippo, Phys. Rev. Lett. **111**, 182001 (2013); Phys. Rev. D **89**, 054506 (2014).

[18] T. Kojo and N. Su, Phys. Lett. B **720**, 192 (2013); **726**, 839 (2013); P. Watson and H. Reinhardt, Phys. Rev. D **89**, 045008 (2014); N. Mueller, J. A. Bonnet, and C. S. Fischer, Phys. Rev. D **89**, 094023 (2014).

[19] G. S. Bali, F. Bruckmann, G. Endrődi, F. Gruber, and A. Schäfer, J. High Energy Phys. 04 (2013) 130; F. Bruckmann, G. Endrődi, and T. G. Kovacs, J. High Energy Phys. 04 (2013) 112.

[20] S. Ozaki, Phys. Rev. D **89**, 054022 (2014).

[21] E. S. Fraga and A. J. Mizher, Phys. Rev. D **78**, 025016 (2008); N. O. Agasian and S. M. Fedorov, Phys. Lett. B **663**, 445 (2008); K. Fukushima and Y. Hidaka, Phys. Rev. Lett. **110**, 031601 (2013).

[22] V. Skokov, Phys. Rev. D **85**, 034026 (2012); K. Fukushima and J. M. Pawlowski, Phys. Rev. D **86**, 076013 (2012); K. Kamikado and T. Kanazawa, J. High Energy Phys. 03 (2014) 009; J. O. Andersen, W. R. Naylor, and A. Tranberg, J. High Energy Phys. 04 (2014) 187.

[23] T. D. Cohen and N. Yamamoto, Phys. Rev. D **89**, 054029 (2014).

[24] N. O. Agasian and I. A. Shushpanov, J. High Energy Phys. 10 (2001) 006; J. Andersen, J. High Energy Phys. 10 (2012) 005; S. Fayazbakhsh, S. Sadeghian, and N. Sadooghi, Phys. Rev. D **86**, 085042 (2012); S. Fayazbakhsh and N. Sadooghi, Phys. Rev. D **88**, 065030 (2013); V. D. Orlovsky and Y. A. Simonov, J. High Energy Phys. 09 (2013) 136.

[25] M. N. Chernodub, Phys. Rev. D **82**, 085011 (2010); Phys. Rev. Lett. **106**, 142003 (2011); M. N. Chernodub, J. Van Doorsselaere, and H. Verschelde, Phys. Rev. D **85**, 045002 (2012).

[26] Y. Hidaka and A. Yamamoto, Phys. Rev. D **87**, 094502 (2013).

[27] E. V. Luschevskaya, O. A. Kochetkov, O. V. Larina, and O. V. Teryaev, arXiv:1411.0730.

[28] C. Bonati, M. D'Elia, M. Mariti, M. Mesiti, F. Negro, and F. Sanfilippo, Phys. Rev. D **89**, 114502 (2014).

[29] M. A. Andreichikov, B. O. Kerbikov, V. D. Orlovsky, and Yu. A. Simonov, Phys. Rev. D **87**, 094029 (2013); H. Liu, L. Yu, and M. Huang, arXiv:1408.1318.

[30] K. Marasinghe and K. Tuchin, Phys. Rev. C **84**, 044908 (2011).

[31] C. S. Machado, F. S. Navarra, E. G. de Oliveira, J. Noronha, and M. Strickland, Phys. Rev. D **88**, 034009 (2013).

[32] J. Alford and M. Strickland, Phys. Rev. D **88**, 105017 (2013).

[33] C. S. Machado, R. D. Matheus, S. I. Finazzo, and J. Noronha, Phys. Rev. D **89**, 074027 (2014).

[34] S. Cho, K. Hattori, S. H. Lee, K. Morita, and S. Ozaki, Phys. Rev. Lett. **113**, 172301 (2014).

[35] R. Rougemont, R. Critelli, and J. Noronha, arXiv:1409.0556; D. Dudal and T. G. Mertens, arXiv:1410.3297.

[36] V. A. Novikov, L. B. Okun, M. A. Shifman, A. I. Vainshtein, M. B. Voloshin, and V. I. Zakharov, Phys. Rev. Lett. **38**, 626 (1977); , Phys. Lett. **67B**, 409 (1977).

[37] M. A. Shifman, A. I. Vainshtein, and V. I. Zakharov, Phys. Rev. Lett. **42**, 297 (1979).

[38] M. A. Shifman, A. I. Vainshtein, and V. I. Zakharov, Nucl. Phys. **B147**, 385 (1979); **B147**, 448 (1979).

[39] M. Shifman, A. Vainshtein, M. Voloshin, and V. Zakharov, Phys. Lett. **77B**, 80 (1978); M. Shifman, Z. Phys. C **4**, 345 (1980).

[40] K. Wilson, Phys. Rev. **179**, 1499 (1969).

[41] L. J. Reinders, H. R. Rubinstein, and S. Yazaki, Phys. Lett. **94B**, 203 (1980); **95B**, 203 (1980).

[42] L. J. Reinders, H. R. Rubinstein, and S. Yazaki, Nucl. Phys. **B186**, 109 (1981).

[43] L. J. Reinders, H. Rubinstein, and S. Yazaki, Phys. Rep. **127**, 1 (1985).

[44] M. A. Shifman, Prog. Theor. Phys. Suppl. **131**, 1 (1998).

[45] S. Narison, *QCD as a Theory of Hadrons* (Cambridge University Press, Cambridge, England, 2004).

[46] A. I. Bochkarev and M. E. Shaposhnikov, Nucl. Phys. **B268**, 220 (1986).

[47] R. J. Furnstahl, T. Hatsuda, and S. H. Lee, Phys. Rev. D **42**, 1744 (1990).

[48] T. D. Cohen, R. J. Furnstahl, D. K. Griegel, and X. Jin, Prog. Part. Nucl. Phys. **35**, 221 (1995).

[49] F. Klingl, S. Kim, S. H. Lee, P. Morath, and W. Weise, Phys. Rev. Lett. **82**, 3396 (1999).

[50] A. Hayashigaki, Prog. Theor. Phys. **101**, 923 (1999).

[51] K. Morita and S. H. Lee, Phys. Rev. Lett. **100**, 022301 (2008).

[52] K. Morita and S. H. Lee, Phys. Rev. C **77**, 064904 (2008).

[53] Y. H. Song, S. H. Lee, and K. Morita, Phys. Rev. C **79**, 014907 (2009).

[54] S. H. Lee and K. Morita, Phys. Rev. D **79**, 011501 (2009).

[55] K. Morita and S. H. Lee, Phys. Rev. D **82**, 054008 (2010).

[56] P. Gubler, K. Morita, and M. Oka, Phys. Rev. Lett. **107**, 092003 (2011).

[57] K. Morita and S. H. Lee, Phys. Rev. C **85**, 044917 (2012).

[58] K. Suzuki, P. Gubler, K. Morita, and M. Oka, Nucl. Phys. **A897**, 28 (2013).

[59] S. H. Lee, K. Morita, T. Song, and C. M. Ko, Phys. Rev. D **89**, 094015 (2014).

[60] T. Hatsuda and S. H. Lee, Phys. Rev. C **46**, R34 (1992); T. Hatsuda, Y. Koike, and S. H. Lee, Phys. Rev. D **47**, 1225 (1993); Nucl. Phys. **B394**, 221 (1993); T. Hatsuda, S. H. Lee, and H. Shiomi, Phys. Rev. C **52**, 3364 (1995).

[61] X. Jin and D. B. Leinweber, Phys. Rev. C **52**, 3344 (1995); S. Leupold, W. Peters, and U. Mosel, Nucl. Phys. **A628**, 311 (1998); S. Zschocke, O. P. Pavlenko, and B. Kampfer, Eur. Phys. J. A **15**, 529 (2002); J. Ruppert, T. Renk, and B. Müller, Phys. Rev. C **73**, 034907 (2006); P. M. Hohler and R. Rapp, Phys. Lett. B **731**, 103 (2014); R. Thomas, S. Zschocke, and B. Kampfer, Phys. Rev. Lett. **95**, 232301 (2005); P. Gubler and K. Ohtani, Phys. Rev. D **90**, 094002 (2014).

[62] A. Hayashigaki, Phys. Lett. B **487**, 96 (2000); T. Hilger, R. Thomas, and B. Kämpfer, Phys. Rev. C **79**, 025202 (2009); T. Hilger, R. Schulze, and B. Kämpfer, J. Phys. G **37**, 094054 (2010); T. Hilger, B. Kämpfer, and S. Leupold, Phys. Rev. C **84**, 045202 (2011); S. Zschocke, T. Hilger, and B. Kampfer, Eur. Phys. J. A **47**, 151 (2011); K. Azizi, N. Er, and H. Sundu, Eur. Phys. J. C **74**, 3021 (2014).

[63] T. Matsui and H. Satz, Phys. Lett. B **178**, 416 (1986).

[64] T. Hashimoto, O. Miyamura, K. Hirose, and T. Kanki, Phys. Rev. Lett. **57**, 2123 (1986).

[65] H. Satz, J. Phys. G **32**, R25 (2006); Nucl. Phys. **A783**, 249 (2007); R. Rapp, D. Blaschke, and P. Crochet, Prog. Part. Nucl. Phys. **65**, 209 (2010), arXiv:0903.1096; R. Rapp and H. van Hees, *Quark-Gluon Plasma 4*, edited by R. C. Hwa and X.-N. Wang (World Scientific, Singapore, 2010).

[66] D. Kharzeev and R. L. Thews, Phys. Rev. C **60**, 041901 (1999); T. Song, C. M. Ko, and S. H. Lee, Phys. Rev. C **87**, 034910 (2013).

[67] Y. S. Oh, S. S. Kim, and S. H. Lee, Phys. Rev. C **65**, 067901 (2002); T. S. Song and S. H. Lee, Phys. Rev. D **72**, 034002 (2005).

[68] S. H. Lee, Y. Park, K.-I. Kim, and T. Song, J. Phys. G **34**, S843 (2007).

[69] S. N. Nikolaev and A. V. Radyushkin, Phys. Lett. **110B**, 476 (1982); **124B**, 243 (1983).

[70] S. N. Nikolaev and A. V. Radyushkin, Nucl. Phys. **B213**, 285 (1983).

[71] L. Reinders, H. Rubinstein, and S. Yazaki, Phys. Lett. **138B**, 425 (1984).

[72] R. A. Bertlmann, Nucl. Phys. **B204**, 387 (1982).

[73] E. Eichten, K. Gottfried, T. Kinoshita, K. D. Lane, and T. M. Yan, Phys. Rev. D **17**, 3090 (1978); **21**, 203 (1980).

[74] Employing the Fock–Schwinger gauge, one would observe that there is no momentum transfer from constant external magnetic fields to traversing quarks when deriving Eq. (B1) for a quark propagator $S_1(x-y)$ with an insertion of an external field. Obviously, this can be extended to a quark propagator $S_n(x-y)$ with an arbitrary number of insertions. A gauge-independent statement follows from a transform property of the quark propagator $S_n(x-y) \to e^{i\alpha(x)} S_n(x-y) e^{-i\alpha(y)}$ in a gauge transformation of an external field $A^\mu_{\rm ext}(x) \to A^\mu_{\rm ext}(x) + \alpha^\mu(x)/|e|$. We thus find that a momentum transfer from an external field to quarks composing a closed loop is exactly zero.

[75] S. C. Generalis and D. J. Broadhurst, Phys. Lett. **139B**, 85 (1984).

[76] S. S. Kim and S. H. Lee, Nucl. Phys. **A679**, 517 (2001).

[77] J. S. Schwinger, Phys. Rev. **82**, 664 (1951).

[78] V. A. Novikov, M. A. Shifman, A. I. Vainshtein, and V. I. Zakharov, Fortschr. Phys. **32**, 585 (1984).

[79] N. Brambilla, P. Pietrulewicz, and A. Vairo, Phys. Rev. D **85**, 094005 (2012); A. Pineda and J. Segovia, Phys. Rev. D **87**, 074024 (2013); A. Pineda, arXiv:1311.3247.

[80] M. Peskin, Nucl. Phys. **B156**, 365 (1979).

[81] G. Bhanot and M. Peskin, Nucl. Phys. **B156**, 391 (1979).

[82] M. E. Luke, A. V. Manohar, and M. J. Savage, Phys. Lett. B **288**, 355 (1992).